Magnetocaloric Materials and the Optimization of Cooling Power Density

Patrick Wikus[a,*], Edgar Canavan[b], Sarah Trowbridge Heine[a], Koichi Matsumoto[c], Takenori Numazawa[d]

[a] *Massachusetts Institute of Technology, Cambridge, MA 02139, USA*
[b] *Code 552, NASA/Goddard Space Flight Center, Greenbelt, MD 20771, USA*
[c] *Department of Physics, Kanazawa University, Kanazawa 920-1192, Japan*
[d] *National Research Institute for Metals, 1-2-1 Sengen, Tsukuba, Ibaraki 305, Japan*

Abstract

The magnetocaloric effect is the thermal response of a material to an external magnetic field. This manuscript focuses on the physics and the properties of materials which are commonly used for magnetic refrigeration at cryogenic temperatures. After a brief overview of the magnetocaloric effect and associated thermodynamics, typical requirements on refrigerants are discussed from a standpoint of cooling power density optimization. Finally, a compilation of the most important properties of several common magnetocaloric materials is presented.

Key words: Magnetocaloric Material, Entropy, ADR, Cooling Power Density

1. MAGNETIC REFRIGERATION

Magnetic refrigeration is employed to provide cooling over many orders of magnitude of temperature, from a few hundred Picokelvin which have been reached with nuclear demagnetization refrigerators [1] to several hundred Kelvin [2, 3]. The magnetocaloric effect, which provides the basis for these refrigeration techniques, is discussed by Shirron [4]. For low temperature applications, the reader's attention is also drawn to Ambler's and Hudson's review of magnetic cooling below 1 K [5].

*Patrick Wikus now works at Bruker Biospin GmbH, Karlsruhe, Germany. Tel: +49 721 5161-6720; e-mail: patrick.wikus@bruker.de

Adiabatic Demagnetization Refrigerators (ADRs) are typically used in the temperature range between a few Millikelvin and a few Kelvin. In this temperature range, ADRs mainly compete with ^{3}He/^{4}He dilution refrigerators and ^{3}He sorption coolers; ADRs have the advantage of more efficient and more accurate temperature control and are thus commonly used to cool low temperature detectors, both in laboratory environments and on spacecraft (e.g. [6, 7]). The thermodynamics of ADRs are described in [8].

In Active Magnetic Regenerators (AMRs), the refrigerant material and the regenerator material are combined into one. This concept allows for the construction of efficient and compact refrigerators. AMRs are being researched for gas liquefaction (e.g. hydrogen [9]), as well as for room temperature refrigeration [10]. The working principle and the thermodynamics of AMRs are described in [11].

The basic principles underlying magnetic refrigeration (with the exception of nuclear demagnetization, which is discussed in [12]) will be reviewed in this introductory section. For more details, reference is made to textbooks such as [13], [14], [15] or [16].

1.1. The Magnetocaloric Effect

The entropy of a magnetocaloric material is the sum of three independent constituents, namely the magnetic entropy S_m, the entropy of the lattice S_l and the entropy of the conduction electrons S_e:

$$S = S_m(B,T) + S_l(T) + S_e(T). \tag{1}$$

The magnitude of all constituents depends on the temperature T, while the magnitude of S_m has an additional strong dependence on the external magnetic field density B. S_l and S_e can be neglected at low temperatures, as S_m is much larger than S_l and S_e combined in that regime.

On a microscopic level, the magnetocaloric effect is caused by the interaction of the external magnetic field with magnetic moments in the material. In most cases, the magnetic moments originate from the presence of unfilled electron shells in transition metal or rare earth ions in the refrigerant, which imparts a total electronic angular momentum J on each ion. The magnetic moments thus have $2J + 1$ possible orientations, and - assuming that the thermal energy k_BT is greater than the splitting between the energy levels of these states - all will be equally occupied and will contribute

$$S_m = R \cdot \ln(2J + 1) \tag{2}$$

to the magnetic entropy, where R is the gas constant (8.314 J mol^{-1} K^{-1}).

If an external magnetic field is applied, the magnetic moments will tend to align with the field, increasing the energy difference between the states, reducing the occupation of higher energy states (those align counter to the field), and thus reducing magnetic entropy. Using statistical mechanics, the field dependence of the magnetic entropy can be derived from the partition function. Assuming that the magnetic moments are completely independent and do not interact with each other, one obtains

$$\frac{S_m}{R} = x\cdot(\coth(x)-(2J+1)\cdot\coth(x\cdot(2J+1)))+\ln\left(\frac{\sinh(x\cdot(2J+1))}{\sinh(x)}\right), \quad (3)$$

where x depends on the temperature T, the magnetic field density B, and properties of the refrigerant.

For a paramagnetic material, x can be calculated with the Bohr magneton μ_B ($9.27\cdot10^{-24}$ J/T), the Boltzmann constant k_B ($1.38\cdot10^{-23}$ J/K) and the Landé g-factor g (an electronic property of the magnetic refrigerant which will be discussed in more detail in section 2.1).

$$x = \frac{\mu_B g B}{2k_B T}. \quad (4)$$

Equations 3 and 4 show that the magnetic entropy of a material depends on the ratio B/T. As B approaches 0, equation 3 will approach equation 2, independent of temperature. In real materials, interaction between ions will always induce some splitting of the energy levels, causing the entropy to approach zero at low temperature. Although these interactions are complex, a rough approximation, useful in ADR design, is to replace B with an effective field B_{eff} in the equations above [13]:

$$B_{\text{eff}} = \sqrt{B^2 + b^2}, \quad (5)$$

where b is a material-dependent parameter.

At low enough temperature, most paramagnetic materials undergo a phase change to an ordered state, usually ferromagnetic or antiferromagnetic (see section 2.2). Entropy drops sharply below the critical temperature. Figure 1 shows the dependence of the entropy S on the magnetic field density B and temperature T for Ferric Ammonium Alum (a common paramagnetic refrigerant). The phase change can be clearly seen by the sharp change in slope at 26 mK.

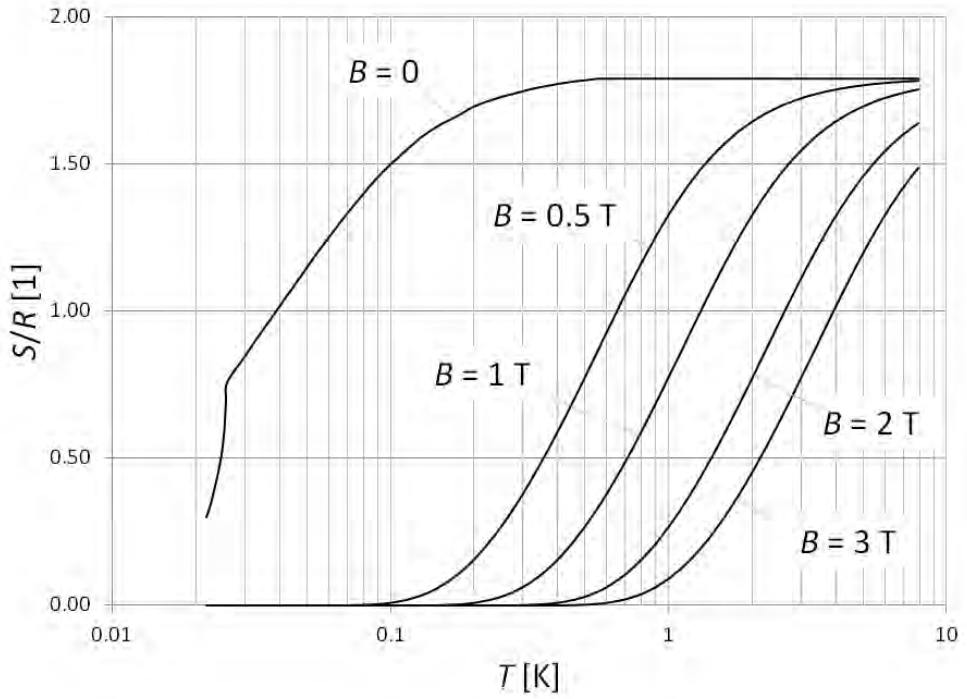

Figure 1: Entropy vs. temperature curves of Ferric Ammonium Alum (FAA) for different values of the external field density B. The entropy is normalized to the gas constant R.

1.2. Thermodynamics of the Magnetocaloric Effect

The magnetocaloric effect can also be described using formalisms from classical thermodynamics. The total differential of the entropy $S(T, B)$ of an isobaric system is

$$dS = \left(\frac{\partial S}{\partial T}\right)_B \cdot dT + \left(\frac{\partial S}{\partial B}\right)_T \cdot dB. \tag{6}$$

In an adiabatic system, $dS = 0$. Using the definition of the specific heat C_B at constant magnetic field,

$$C_B = T \cdot \left(\frac{\partial S}{\partial T}\right)_B, \tag{7}$$

and Maxwell's relation for the magnetization M,

$$\left(\frac{\partial S}{\partial B}\right)_T = \left(\frac{\partial M}{\partial T}\right)_B, \tag{8}$$

one obtains the following relation for the adiabatic temperature change dT/dB, which is often used to characterize the magnitude of the magnetocaloric effect:

$$\frac{dT}{dB} = -\frac{T}{C_B} \cdot \left(\frac{\partial M}{\partial T}\right)_B. \tag{9}$$

Equation 9 shows that the magnetocaloric effect is large if the temperature T is high, if the specific heat C of the refrigerant is small, and if the magnetization changes rapidly with temperature; the latter condition is fulfilled around magnetic phase transitions in the refrigerant.

Knowledge of entropy as a function of temperature and magnetic field is essential for the design of magnetic coolers, and the above relations are useful in determining entropy from measurements of refrigerant properties. Measurements of either the specific heat $C(T, B)$ or the magnetization $M(T, B)$ allow the calculation of ΔS_B. It is not possible to measure the three constituents of the entropy (magnetic, lattice and electronic) separately; only the total entropy change ΔS_B is accessible by experiment.

If the specific heat $C(T, B)$ is measured on a sample of a magnetocaloric material, the entropy can be derived with the following equation:

$$S(T, B) = \int_0^T \left(\frac{C(T', B)}{T'}\right)_B dT'. \tag{10}$$

In some cases, it is difficult to measure the specific heat to temperatures low enough such that $C(T', B)$ can be easily extrapolated to $T = 0$. Then, the entropy from equation 10 is best separated into two parts,

$$S(T, B) = \int_0^{T_0} \left(\frac{C(T', B)}{T'}\right)_B dT' + \int_{T_0}^T \left(\frac{C(T', B)}{T'}\right)_B dT', \tag{11}$$

where T_0 is the lowest temperature achieved in the specific heat measurements. Usually, the specific heat data at high magnetic fields can be extrapolated to $T = 0$, because the specific heat peak due to phase transitions is suppressed in high fields. For many materials, the specific heat can be extrapolated with a T^3 dependence for the lattice entropy and a linear dependence on T for the electronic specific heat.

If the magnetization is measured, the change in magnetic entropy induced by field B, $\Delta S(T,B) = S(T,B) - S(T,0)$, can be calculated by integrating the Maxwell relation (equation 8), which gives

$$\Delta S(T,B) = \int_0^B \left(\frac{\partial M}{\partial T}\right)_{B'} \cdot dB'. \tag{12}$$

ΔS can then be computed by integrating the partial differentials of the magnetization M with respect to the temperature T from zero to the magnetic field B. The entropy change ΔS can be calculated for both the magnetization and demagnetization process. Rewriting the Maxwell relation for two sufficiently close temperatures T_1 and T_2 yields

$$\Delta S(T,B) = \int_0^B \left(\frac{M(T_1) - M(T_2)}{T_1 - T_2}\right)_{B'} \cdot dB' = \\ = \frac{1}{T_1 - T_2} \int_0^B (M(T_1) - M(T_2)) \cdot dB'. \tag{13}$$

Thus, the entropy change can be obtained from the area between two magnetization curves at different temperatures. Magnetization measurements can be performed very accurately with SQUID magnetometers.

Note that the magnetization technique only yields $\Delta S\,(T,B)$. Full determination of $S\,(T,B)$ still requires some specific heat data, to determine at least one total entropy vs. temperature curve.

Determination of ΔS by these two methods usually yield identical results for paramagnetic or soft magnetic materials. For materials with first order phase transitions, the results obtained with the two methods sometimes differ from each other, however. The latent heat associated with the first order phase transition causes a discontinuity in the specific heat data.

1.3. ADR Cycle (Carnot Cycle)

Adiabatic Demagnetization Refrigerators (ADRs) will be discussed here as an example of refrigerators employing the magnetocaloric effect. Details of another popular magnetic refrigeration concept, the Active Magnetic Regenerator (AMR) Refrigerator, are discussed elsewhere [17, 18]. Regenerative thermal cycles - such as AMRs - are mainly used at temperatures above approximately 15 K, where high cooling power densities cannot be achieved

with the Carnot cycle due to the exceedingly large contribution of the lattice entropy to the total entropy (for details, see section 2.3).

ADRs use the magnetocaloric effect to lift heat from an object at temperature T_{cold} to a heat sink at T_{hot} using the Carnot cycle. The cycle is shown in Figure 2. This entropy-temperature diagram shows various entropy curves for a paramagnetic refrigerant (FAA) for different external magnetic field densities.

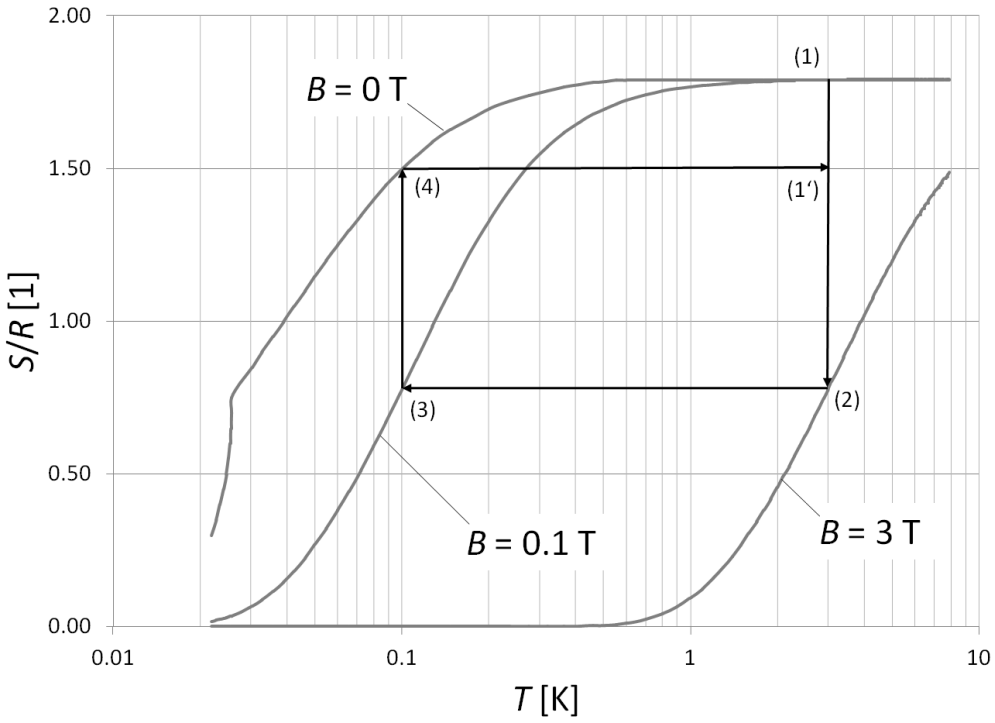

Figure 2: The T-S diagram of a typical ADR cooling cycle. With an ADR, the ideal Carnot cycle can be approximated very closely. The entropy is normalized to the gas constant R.

In a typical refrigeration cycle, the paramagnetic salt is first thermally connected to a heat sink with temperature T_{hot} (3 K in the example in Figure 2); the magnetic field is then increased (from 0 to 3 T in our example). In the T-S diagram, this corresponds to the magnetization (1)→(2). The heat sink must absorb the energy

$$Q_{\text{hot}} = T_{\text{hot}} \cdot (S_1 - S_2) = T_{\text{hot}} \cdot \Delta S_{\text{hot}}. \tag{14}$$

The thermal connection to the heat sink is then open, leaving the salt thermally isolated. The magnetic field is then decreased, corresponding to adiabatic demagnetization from 3 T to 0.1 T; this corresponds to (2)→(3) in Figure 2. During this step, the refrigerant cools down to T_{cold} - from 3 K to 0.1 K in our example. In a real system, it is of course impossible to achieve perfect thermal insulation of the refrigerant. Achieving good thermal insulation is one of the key design drivers for refrigerant suspension systems [19].

Once the desired temperature is achieved, the rate of decrease of the magnetic field is controlled to maintain constant temperature, so that the heat absorption by the refrigerant just balances the heat flux from the load; this corresponds to (3)→(4) in Figure 2. During this isothermal process, the refrigerant absorbs heat

$$Q_{\text{cold}} = T_{\text{cold}} \cdot (S_4 - S_3) = T_{\text{cold}} \cdot \Delta S_{\text{cold}}. \tag{15}$$

In our example, this isothermal demagnetization is performed until the external field reaches zero. The refrigerant is then disconnected from the cold reservoir, and the magnetic field is ramped up until the refrigerant's temperature corresponds to the temperature of the heat sink, (4)→(1'). The cycle can then start over with the isothermal magnetization.

Note that once heat sink temperature and maximum field are set, the heat absorbed per cycle is a simple function of T_{cold}.

The cooling power P of the ADR refrigeration cycle is proportional to the frequency f of the cycle:

$$P = f \cdot Q_{\text{cold}} = f \cdot T_{\text{cold}} \cdot \Delta S_{\text{cold}}. \tag{16}$$

The cycle frequency f is limited by thermal resistances between the refrigerant and the heat sink, and between the refrigerant and the cold load, respectively. Because of these resistances, entropy is generated in flowing heat into and out of the refrigerant, reducing the efficiency of the cycle as the frequency increases. The minimization of the thermal resistance between the refrigerant and the cold reservoir is thus key for optimizing performance; this is discussed in section 4.

The Coefficient Of Performance (COP) of a thermodynamic cycle is the ratio of the cooling power Q_{cold} to the work $Q_{\text{hot}} - Q_{\text{cold}}$ which needs to be performed to achieve the cooling:

$$\mathrm{COP} = \frac{Q_{\mathrm{cold}}}{Q_{\mathrm{hot}} - Q_{\mathrm{cold}}}; \tag{17}$$

in the Carnot cycle, this is equivalent to

$$\mathrm{COP}_{\mathrm{ideal}} = \frac{T_{\mathrm{cold}}}{T_{\mathrm{hot}} - T_{\mathrm{cold}}}. \tag{18}$$

For an ideal ADR operating between 0.05 K and 2 K, the COP amounts to 0.026. The thermodynamic efficiency of a real cycle can then be defined as the ratio of the COP of the real cycle to the COP of the ideal Carnot cycle operating between the same two temperatures:

$$\eta = \frac{\mathrm{COP}}{\mathrm{COP}_{\mathrm{ideal}}}. \tag{19}$$

1.4. Important Properties of Magnetocaloric Materials

To be useful for the construction of efficient magnetic refrigeration systems, refrigerants need to fulfill certain requirements. Yu, for instance, has summarized these requirements for AMRs [20].

To achieve a high cooling power density, the material should exhibit a large magnetocaloric effect in the temperature range in which the system operates. A large magnetocaloric effect is achieved if

- the total angular momentum number J and the Landé factor g are large;
- the refrigerant's ordering temperature is sufficiently close to the temperature range in which the system operates to profit from a large $\partial M/\partial T$, but sufficiently far away to avoid the spontaneous entropy reduction brought about by the magnetic ordering.

In addition, to allow high operating frequencies f and, in consequence, large cooling powers, the magnetic material should exhibit

- small magnetic and thermal hysteresis;
- a large electrical resistance to keep eddy current heating low;
- a large thermal conductivity to minimize temperature gradients.

Furthermore, certain practical requirements exist: The refrigerant must be commercially available, and its cost must be reasonable. It is desirable that the material is non-toxic, does not corrode, and that the manufacturing process which is required to bring the refrigerant into the form in which it will be used in the system (e.g. crystal growing or sintering) is a simple one. In addition, it is desirable that a simple method exists to make good thermal contact to the refrigerant.

Unfortunately, some of these requirements contradict each other; high thermal conductivity often goes hand in hand with high electrical conductivity, for instance.

2. OPTIMIZATION OF COOLING POWER DENSITY

Usually, the magnetocaloric material for a specific application is chosen such that the cooling power density of the entire system is maximized. The optimization process needs to take into account both the magnet and the refrigerant. In most cases, the magnet and associated shielding dominates the mass and volume of the refrigeration system, but the magnet mass is proportional to the volume of the refrigerant. Thus, the usual design goal is the minimization of the refrigerant size. In non-continuous, or "single shot", ADRs, cooling capacity (cooling power times hold time) sets a lower limit on the amount of refrigerant. Since large magnetic field changes facilitate high cooling power densities, superconducting magnets are usually used. However, because critical current drops with increasing field, the mass of a superconducting solenoid increases faster than linearly with field, and, thus, there is an optimum field strength.

Various optimization criteria for magnetocaloric materials have been proposed; Wood and Potter [21] suggest choosing refrigerants that maximize the product $(T_{\mathrm{hot}} - T_{\mathrm{cold}}) \cdot \Delta S_{\mathrm{cold}}$ that can be achieved with a given thermodynamic cycle. Wood and Potter call this product "refrigerant capacity". They argue that in magnetic refrigeration, $(T_{\mathrm{hot}} - T_{\mathrm{cold}})$ and ΔS_{cold} cannot be chosen independently from each other for a given magnetic field excursion, and that it consequently does not make sense to maximize one or the other individually. Also, with equation 15,

$$(T_{\mathrm{hot}} - T_{\mathrm{cold}}) \cdot \Delta S_{\mathrm{cold}} = Q_{\mathrm{cold}} \cdot \frac{T_{\mathrm{hot}} - T_{\mathrm{cold}}}{T_{\mathrm{cold}}} \tag{20}$$

i.e. Wood's and Potter's criterion maximizes the product of the heat that can

be absorbed at T_{cold} and the fractional temperature span across which the heat has to be pumped. Yet another interpretation of Wood's and Potter's criterion is that it maximizes the heat Q_{cold} that can be absorbed per COP point (see equation 18).

Here, an alternative optimization criterion is proposed, namely the maximization of $\Delta S_{\mathrm{cold}} = Q_{\mathrm{cold}}/T_{\mathrm{cold}}$ per COP point. In cryogenic applications, where T_{hot} is often much larger than T_{cold}, the optimization criterion can be simplified:

$$Q_{\mathrm{cold}} \cdot \frac{T_{\mathrm{hot}} - T_{\mathrm{cold}}}{T_{\mathrm{cold}}^2} = \Delta S_{\mathrm{cold}} \cdot \frac{T_{\mathrm{hot}} - T_{\mathrm{cold}}}{T_{\mathrm{cold}}} \approx \Delta S_{\mathrm{cold}} \cdot \frac{T_{\mathrm{hot}}}{T_{\mathrm{cold}}}. \qquad (21)$$

2.1. Ions and ion density

An important factor in maximizing cooling power density is the use of materials with large zero-field magnetic entropy, so that the application of a magnetic field can result in a large entropy change. Equation 2 indicates that the total angular momentum J should thus be as large as possible.

Hund's rules [22, 23] can be used to estimate the total angular momentum J of rare earth ions. The electrons' spin angular momentum S (not to be confused with the entropy S used above) and the orbital angular momentum L couple weakly via spin-orbit interactions; as a consequence, the two angular momenta are not conserved separately, but - following Hund's 3^{rd} rule - are conserved as the total angular momentum $J = |L + S|$ if the electron shell is more than half full, and as $J = |L - S|$ if the electron shell is less than half full.

For example, the Ce^{3+} ion has a [Xe] $4f^1$ electron configuration; the azimuthal quantum number l is 3 for the f sub-shell. In accordance with Hund's 1^{st} rule, the spin of a single electron in a subshell must be parallel, i.e. $S = 1/2$. To satisfy Hund's 2^{nd} rule, the orbital angular momentum must be maximized, and thus $L = 3$ ($L = \sum m_l$, where m_l is the magnetic quantum number and ranges from $-l$ to l). The total angular momentum of an isolated Ce^{3+} ion is finally given by Hund's 3^{rd} rule, $J = |L - S| = 5/2$. However, interactions with the crystal field, the electric field due to neighboring ions, can lead to partial lifting of degeneracies of ground multiplets. The Kramers degeneracy theorem [24] states that systems with an odd total number of electrons remain at least doubly degenerate in the absence of magnetic fields. These pairs of degenerate states are called Kramers doublets. For instance, in Cerium Magnesium Nitrate (CMN), a paramagnetic

salt commonly used for very low temperature cooling and thermometry, the $J = 5/2$ ground multiplet of the Ce^{3+} ions is split into three Kramers doublets [25]. At low temperature, only the lowest doublet is populated, and thus CMN is best described as a $J = 1/2$ material.

Hund's rules predict experimental results very well for rare earths, as their partially filled 4f shells lie deep within the ion, and have weaker interaction with the crystal field. For the iron group transition metals, or 3d ions, Hund's rules do not yield satisfactory results, and molecular field theory must be used. The failure of Hund's rules is mainly due to interactions between the electrons in the 3d sub-shell and the surrounding crystal field, which dominate spin-orbit interactions [26].

Experimental data suggests that 3d systems assume a ground state such that $J = S$, an effect which is called "orbital quenching" [26]. Examples for transition metals which have been used successfully in magnetic refrigeration include the ions Fe^{3+} in the paramagnetic salt FAA ($J = 5/2$), Cr^{3+} in CPA ($J = 4/2$), and Mn^{2+} in MAS ($J = 5/2$).

Gadolinium is a special case. In Gadolinium, the 4f sub-shell is half full, and the orbital angular momentum L vanishes as a result of Hund's 1^{st} and 2^{nd} rules. Hence $J = S = 7/2$, the largest of any ion [27]. Moreover, there is no distortion of the spherical 4f charge density, and consequently little interaction with the crystal field. Thus, Gadolinium compounds typically have the magnetic entropy $S_m = R \cdot \ln(8)$ predicted for a fully degenerate $J = 7/2$ shell, and are often used in magnetic refrigeration.

The contribution of spin angular momenta to the magnetic moment of an atomic electron is characterized by the Landé g-factor g, which is defined as

$$g = 1 + \frac{J(J+1) + S(S+1) - L(L+1)}{2J(J+1)}; \tag{22}$$

equation 22 does not hold if spin-orbit interactions are not the main type of coupling. Thus, in the iron group transition metal ions, $g \approx 2$. For a magnetic refrigerant, the Landé g-factor should be as large as possible to maximize cooling power density.

Dysprosium compounds have very high g-factors, which can also exhibit spacial anisotropy. Dysprosium Gallium Garnet (DGG), for instance, has a g-factor of 8 and Dysprosium Aluminum Oxide (DOA) a g-factor of 14; for comparison, CMN, FAA, CPA and MAS all have a g-factor of 2. In addition, the net magnetic moment of DOA varies greatly with the crystal orientation; it is almost one order of magnitude larger along the [010] axis

than along the [001] axis. Kuzmin [28] proposed to use this anisotropy to create a refrigerator in which the refrigerant simply rotates in a constant magnetic field.

Naturally, materials with greater density of magnetic ions have higher cooling power density. The ion densities for several common refrigerants are listed in Tables 1 and 2. A higher concentration means a shorter distance between the magnetic ions, and hence stronger interaction and higher ordering temperature. The correlation between ion density and ordering temperature is illustrated in Figure 3. The correlation is not perfect because non-magnetic ions and the type of bond influence the strength of the interactions. For example, metals generally have higher ordering temperatures than ionic compounds because of the Ruderman-Kittel-Kasuya-Yoshida (RKKY) interaction [29, 30, 31]. In a metal, localized magnetic moments spin-polarize the electron gas, which in turn then interacts with other magnetic moments. The resulting indirect interaction between magnetic moments gives rise to a higher ordering temperature.

Thus, more dilute salts must be used for cooling to lower temperatures. Well known compounds include the hydrated salts CMN, CPA, MAS and FAA, which have often been used at to achieve temperatures below 100 mK. Gadolinium chloride elpasolite (GCE, $Cs_2NaGdCl_6$) is an attractive candidate material because of its its low ordering temperature of 35 mK, in spite of its rather high ion density [32]. Unfortunately, $Cs_2NaGdCl_6$ is deliquescent and consequently difficult to handle, and has not yet been used in a practical ADR. The Gadolinium fluoride elpasolite (Cs_2NaGdF_6) is hydrophobic and expected to have magnetic properties which are similar to the ones of $Cs_2NaGdCl_6$. At higher temperatures, fluorides and oxides (such as GGG, GLF or GdF) are often employed as refrigerants. High-spin molecular clusters such as Mn_{12} or Fe_8 have recently been suggested for helium liquefaction [33].

2.2. Magnetic Ordering

The minimum temperature which can theoretically be achieved by adiabatic demagnetization of a magnetocaloric material is determined by the material's ordering temperature, where a transition occurs and the magnetic moments align spontaneously. This results in a reduction of the magnetic entropy to zero over a very small temperature range, or - in other words - a small entropy change over a large range of magnetic field densities. The temperature at which this ordering occurs is called Curie temperature T_C if

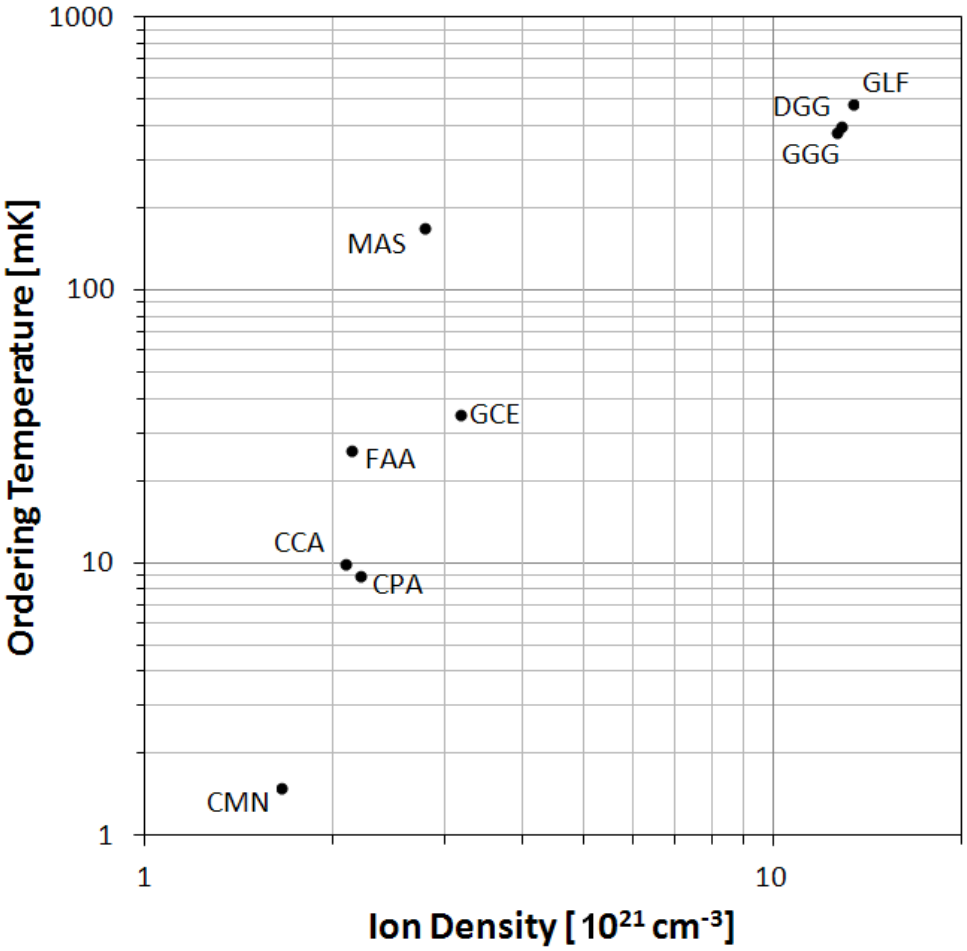

Figure 3: Interactions between paramagnetic ions are largely proportional to a refrigerant's ion density; larger interactions between ions result in higher ordering temperatures and limit the minimum temperature at which a material can be used for refrigeration.

the magnetocaloric material undergoes ordering from the paramagnetic to the ferro- or ferrimagnetic state, and Néel temperature T_N if the ordering goes from the paramagnetic to the antiferromagnetic state.

In accordance with equation 9, the magnetocaloric effect is large when the derivative of the magnetization with respect to temperature $(\partial M/\partial T)_B$ is large; this is the case in the vicinity of magnetic order-disorder phase transitions. In magnetocaloric materials, ferromagnetic interaction is preferable

to antiferromagnetic interaction, as the applied external magnetic field is enhanced by the internal field.

Some paramagnetic materials, such as Gadolinium Gallium Garnet (GGG, see section 3.2), do not undergo a transition to an ordered phase. In GGG, no long range magnetic order has been observed down to 25 mK in the absence of external magnetic fields [34]. This is attributed to geometric frustration of the spins [35]; the magnetic ions are positioned on well-ordered points in the lattice structure such that interactions between the magnetic moments preclude the existence of one single preferred spin orientation. Geometric frustration thus leads to a large number of possible ground states and suppresses magnetic ordering. The temperature below which frustration induced spin freezing occurs in GGG is estimated to be 130 mK. In the presence of a magnetic field, GGG undergoes antiferromagnetic ordering (at a field of 1 T, the Néel temperature T_N is 380 mK) [36]. Due to the presence of a large number of soft modes, the magnetocaloric effect is enhanced in geometrically frustrated systems [37].

2.3. Lattice Entropy

The lattice entropy S_l can be calculated from the lattice specific heat C_l,

$$S_l(T) = \int_0^T \frac{C_l(T')}{T'} \cdot dT'. \tag{23}$$

Assuming that the temperature T is small compared to the Debye temperature θ_D,

$$S_l(T) \propto \int_0^T \frac{T'^3}{T'} \cdot dT' \propto T^3. \tag{24}$$

Due to the lattice entropy's T^3 dependence, the contribution of the lattice to the total entropy (see equation 1) cannot be neglected at higher temperatures; for typical refrigerants, this occurs at around 15 K.

In a magnetic refrigerator, the magnet sets practical limits to the maximum achievable variation of the magnetic field. A non-negligible lattice entropy S_l reduces the contribution of the magnetic entropy S_m to the total entropy $S = S_m + S_l + S_e$; in that case, a given change of the external magnetic field decreases the total entropy less than would be the case if the total entropy consisted only of the magnetic term ($S = S_m$). As a consequence, the magnetic field needs to be ramped down more to achieve a certain base

temperature (step (2)→(3) in the description of the cycle in section 1.3), and less field is available for the isothermal absorption of Q_{cold} (step (3)→(4)). In other words, the lattice entropy adds a significant slope to the lines of constant field in Figure 2, which greatly reduces the temperature change achievable by adiabatic demagnetization from a point at a given field and temperature in this region.

As a consequence, the lattice entropy should be as small as possible to maximize the cooling power density. At temperatures below 15 K, where the lattice entropy is relatively small, the Carnot cycle can be employed effectively and paramagnetic salts and rare-earth oxides with low magnetic ordering temperatures are commonly used.

In some materials, the entropy of the lattice can even contribute to the cooling power. This behavior was first observed in 1997 in the compound $Gd_5Si_2Ge_2$, and is called "Giant Magnetocaloric Effect" [38]. The giant magnetocaloric effect is attributed to field-induced structural transformations of the crystal. When the external field changes, the entropy difference between the two structures (which is a change in the lattice entropy) adds to the magnetic entropy change, and amplifies the conventional magnetocaloric effect [39].

3. MATERIAL DATA

A vast number of materials has been studied with respect to their suitability for magnetic refrigeration. While paramagnetic salts with operating temperatures of a few Kelvin and below were investigated intensively in the mid-twentieth century, the research focus has now largely shifted towards rare-earth compounds for refrigeration between 15 K and room temperature.

3.1. Hydrated Paramagnetic Salts

Hydrated paramagnetic salts contain ions with only partially filled electron shells. The large distance between the ions (which is required for a low ordering temperature) is due to the large amount of water of crystallization in the salt. In the following, the paramagnetic salts which are most commonly used for refrigeration are described, sorted by increasing ordering temperature.

Cerium Magnesium Nitrate (CMN) is a popular magnetic refrigerant because of its low ordering temperature of just below 2 mK [40]. The crystals contain a large amount of water, which assures a large distance between the

magnetic Ce^{3+} ions (about 1 nm). The ions' distance from each other leads to weak interactions between them [41], contributing to a small internal magnetic field b (cf. equation 5) and a low T_c. The heat capacity of CMN has been measured between 0.6 mK and 4.2 K by Fisher et al. [42]. Crystal growth is complicated because the solubility of CMN is a strong function of temperature so care is required during growth and properties may vary between samples produced in different environments [43]. In experiments where it can be in direct contact with liquid helium, CMN is often used in powdered form, which affords an advantage for heat transfer because of the larger surface area. The powdered form is especially popular with ^{3}He experiments because CMN has an anomalously low Kapitza resistance with ^{3}He [44, 45]. However, the susceptibility of CMN is strongly anisotropic so that individual crystallites oriented in different directions with respect to the magnetic field can cool to dramatically different temperatures. Establishment of thermal equilibrium through grain to grain heat transfer is inefficient and has the same effect as a relatively large but decreasing heat leak [43]. CMN is also often used for the construction of magnetic thermometers in which the magnetic susceptibility of a material is measured to determine the absolute temperature in accordance with the Curie-Weiss law. CMN (CAS number 13550-46-4) is currently difficult to obtain commercially. At the time of writing, no industrial suppliers could be found.

Lanthanum Cerium Magnesium Nitrate (LCMN) is a modified version of CMN where some of the magnetic Ce^{3+} ions are replaced by non-magnetic Lanthanum ions. This reduces the internal magnetic field b further and thus the magnetic ordering and base temperatures. Temperatures below 1 mK were achieved in demagnetization experiments of compressed LCMN powder samples with 90 percent of the ion sites occupied by La rather than Ce atoms. However, due to contributions to the internal magnetic field b aside from the magnetic dipole interaction of the magnetic ions, dilution cannot eliminate the internal magnetic field completely [46].

Chromium Potassium Alum (CPA) has a long history of use in magnetic cooling experiments with its use dating back to 1933 [47]. Its heat capacity was measured between 30 mK and 0.8 K by Vilches and Wheatley [48, 49] and between 1 K and 4.2 K by Kapadnis [50]. It has a relatively low ordering temperature of 10 mK [13], and its octahedral crystals can be easily grown to large sizes [43]. Unlike CMN and LCMN, its magnetic susceptibility is isotropic so that it can be used in powder form with no less cooling power than in its crystalline form [43]. As with many hydrated salts, CPA loses

its water of crystallization quite easily and so must be sealed well for use in vacuum. It does not attack copper, and so can be grown on a copper, rather than gold, thermal bus. CPA is readily availably as small crystals from several suppliers of laboratory chemicals at a comparatively low price (CAS RN 7788-99-0).

Ferric Ammonium Alum (FAA) is one of the most commonly used paramagnetic refrigerants. The specific heat of FAA was measured by Vilches and Wheatley [48], who also observed magnetic ordering at 26 mK. FAA is readily availably in crystalline form (CAS RN 7783-83-7). FAA readily dissolves copper, and has even been known to dissolve away the copper wires inside gold plating. As a consequence, in ADR salt pills using FAA, the crystals are grown around bundles of gold wires, and the hermetic enclosures are typically constructed from 316 stainless steel. FAA breaks down when subjected to temperatures in excess of approximately 35 °C, so one must be careful to store FAA salt pills in a temperature-controlled environment, particularly in warm climates.

Manganese Ammonium Sulfate (MAS) has a magnetic ordering temperature of 170 mK [13] so is more popular cooling samples in higher temperature ranges. It is part of the family of Tutton salts, which contain two different cations similar to the alums, but with a slightly different chemical formula. Like CPA and FAA, its susceptibility is isotropic so it can be used in powdered form with little loss of cooling power. Its entropy has been measured by Vilches et al. [48, 49] down to 90 mK.

3.2. Rare-Earth Oxides and Fluorides

Due to their chemical stability and high magnetic ion concentration, rare-earth oxides have been studied intensively. Rare earth garnets are used in hydrogen liquefaction applications as they do not hydrogenate. Barclay [51] gives a comprehensive compilation of various Gd compounds.

Gadolinium Gallium Garnet (GGG, $Gd_3Ga_5O_{12}$, CAS RN 12024-36-1) has been used as the working material in magnetic refrigerators in the temperature range from 2.0 to 20 K for the production of superfluid helium and for liquefying helium [52]. Good quality crystals with high thermal conductivity and chemical stability can be produced at reasonable cost. The entropy change of GGG becomes small at high temperatures, however. Entropy values for GGG were published by many authors, for instance by Fisher et al. [53]. The g-factor of GGG is isotropic and amounts to 2.

Dysprosium Aluminum Garnet (DAG, $Dy_3Al_5O_{12}$) is a magnetocaloric material which facilitates higher cooling power densities than GGG; this is due to a strong anisotropic magnetic interaction of the Dy ion. The g-factors of single DAG crystal are 10.6, 8.8 and 6.5 for the <111>, <110> and <100> directions, respectively.

Figure 4[1] shows entropy diagrams for single crystals of GGG and DAG with the magnetic field in the <111> direction [54]. The zero-field saturation entropy is higher for GGG than for DAG, as the Gd ion in the GGG has a magnetic moment of $J = 7/2$, while the degeneracy of the large room temperature magnetic moment of the Dy ion in DAG is lifted by the crystal field at low temperatures, leaving only an effective magnetic moments of $J = 1/2$ due to a Kramers doublet. As the figure shows, at temperatures above 10 K, DAG provides a larger entropy change than GGG because of its larger g-factor, which directly multiplies magnetic field in the entropy function (equations 3 and 4).

When polycrystalline DAG is used as a refrigerant, the strong anisotropy of Dy must be taken into account. In polycrystalline DAG, the crystals are randomly oriented, and the anisotropic effect is averaged. The entropy change of polycrystalline DAG roughly decreases to the level of the single crystal along the <110> direction.

The thermal conductivity of many single crystal garnets - including the two refrigerants discussed above, GGG and DAG - was measured by Slack and Oliver [55]. In general, the thermal conductivity of GGG is typical for single crystal dielectrics, with a strong peak in the 10 to 30 K range. The peak for DAG is smaller and occurs at lower temperature, possibly because of phonon scattering produced by low-lying electronic levels of the Dy ion.

Gadolinium Dysprosium Aluminum Garnet (GDAG), i.e. DAG with a partial substitution of Dy with Gd, has been studied to solve the anisotropy problem of DAG [56, 57]. Figure 5 shows the entropy change for the polycrystalline $(Gd_xDy_{1-x})_3Al_5O_{12}$ samples (x = 0, 0.1 and 0.2) and monocrystalline DAG in the magnetic field of 6 T [54]. The substitution of Dy with Gd increases the magnetic entropy change and therefore the total entropy,

[1] In Figure 4 and most of the following plots, the material data is given per unit mass, as this value can be measured reliably. The entropy and specific heat per unit volume depend on the mass density of the material, which is influenced by the manufacturing process and may vary between samples. In the following, entropy per unit volume will only be shown if the relative density of the sample was well known.

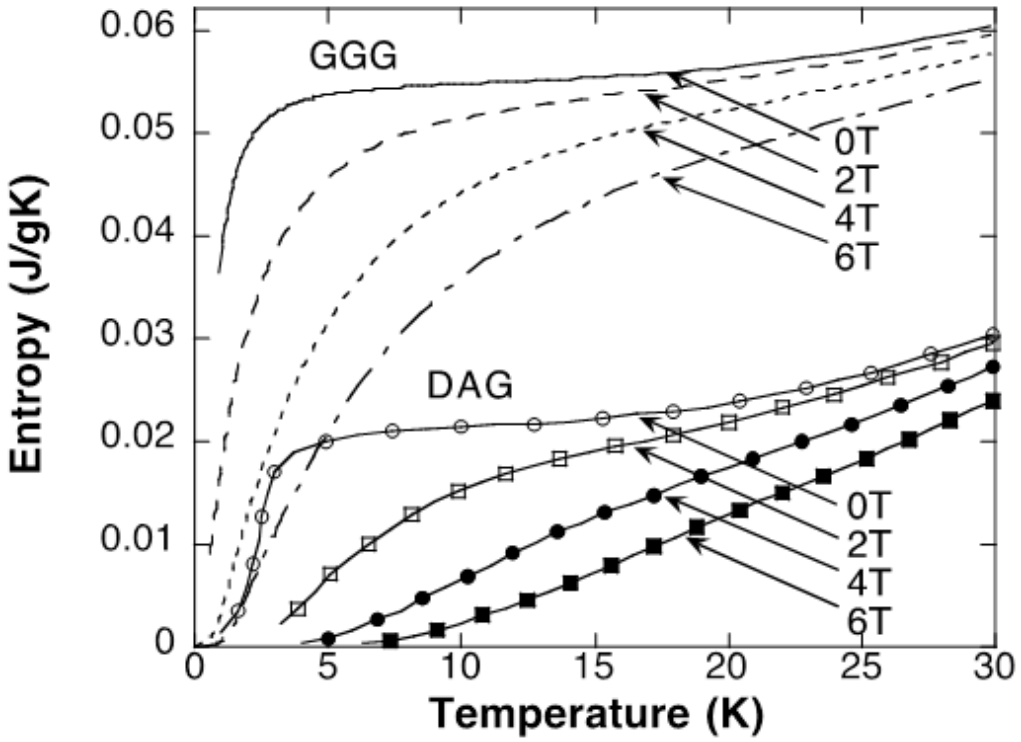

Figure 4: Entropy diagram of single crystals of GGG and DAG for the magnetic fields of 0, 2, 4 and 6 T [54].

especially in the liquid hydrogen temperature range of about 20 K.

For practical purposes, it is important that a magnetocaloric material is available in various shapes such as plates and small spheres. As a consequence, polycrystalline rectangular solid and spherical particles of GDAG were made and tested to confirm that the production process did not influence the magnetic properties in a negative way [58, 59]. Figure 6 shows GDAG shaped into a 10 cm size plate and small spheres with 0.4 mm diameter, with 99.5 percent relative density and a Vickers hardness of 500. The diameters found in the spherical material stay within 10 percent of the average value of 0.4 mm.

Gadolinium Gallium Iron Garnet (GGIG) is an Fe-modified Gd-Ga nanocomposite garnet. It was demonstrated that when iron is added to the garnets in substitution for some of the gallium atoms, the resulting magnetocaloric

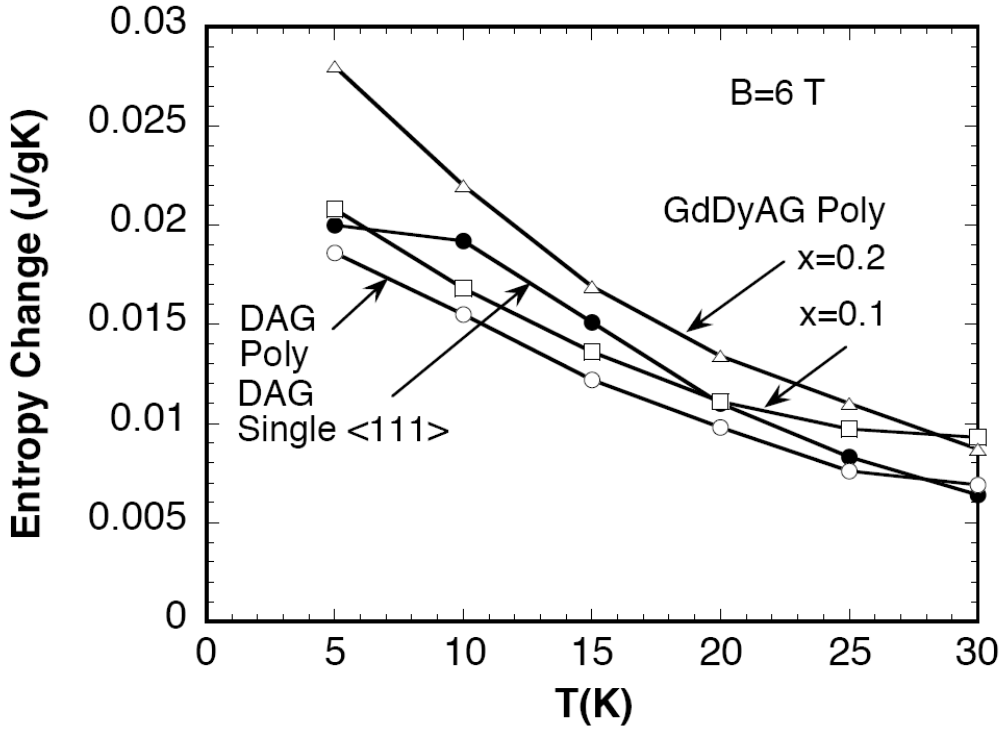

Figure 5: Entropy change of polycrystalline $(Gd_xDy_{1-x})_3Al_5O_{12}$ samples for x = 0, 0.1 and 0.2 in comparison with monocrystalline DAG [54].

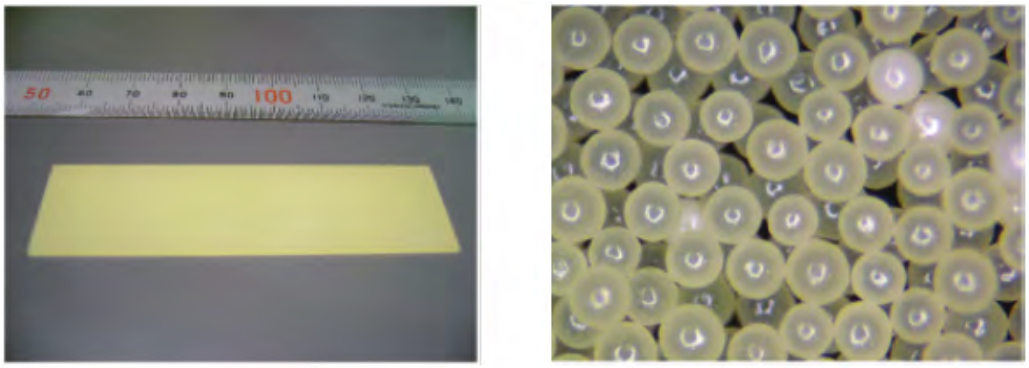

Figure 6: Photographs of a rectangular solid and spherical particles of GDAG.

response is increased in comparison to the garnets without the iron addition [60, 61, 62, 63]. The magnetic entropy changes ΔS of GGG and GGIG

($Gd_3(Ga_{1-x}Fe_x)_5O_{12}$) with x = 0.125, 0.25, 0.4 and 0.5 induced by an external field of 5 T are shown in Figure 7 [63].

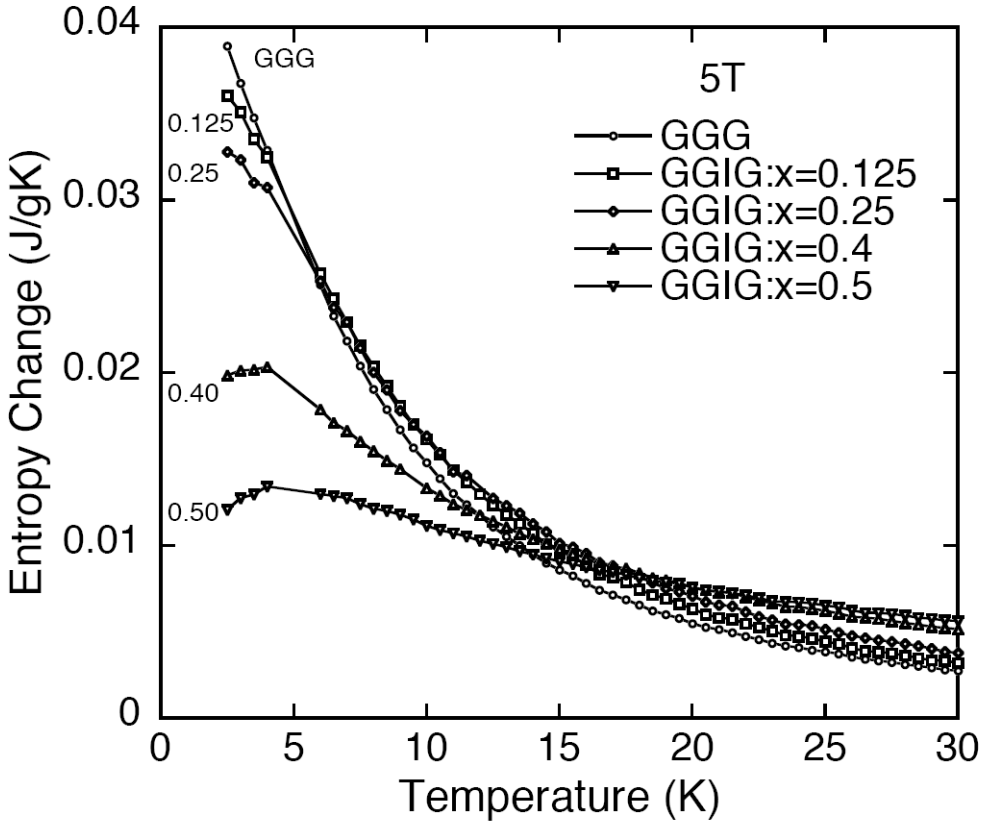

Figure 7: Magnetic entropy change ΔS of GGG and GGIG ($Gd_3(Ga_{1-x}Fe_x)_5O_{12}$) with x = 0.125, 0.25, 0.4 and 0.5 induced by an external field of 5 T. ΔS was calculated from magnetization data [63].

Figure 8 shows the entropy diagram for GGIG with the comparatively high iron content of $x = 0.4$ [63] for various magnetic fields. The entropy of GGIG with $x = 0.4$ increases smoothly at low temperature, and has a larger slope than the entropy of GGG at high temperature. This tendency becomes more pronounced with increasing iron content. GGIG with a high iron content is thus unsuitable for refrigerators using the Carnot cycle because the adiabatic temperature change is small. The most suitable cycles for GGIG with high iron content are regenerative thermal cycles such as Stirling, Ericsson, and the Active Magnetic Regenerator (AMR) cycle.

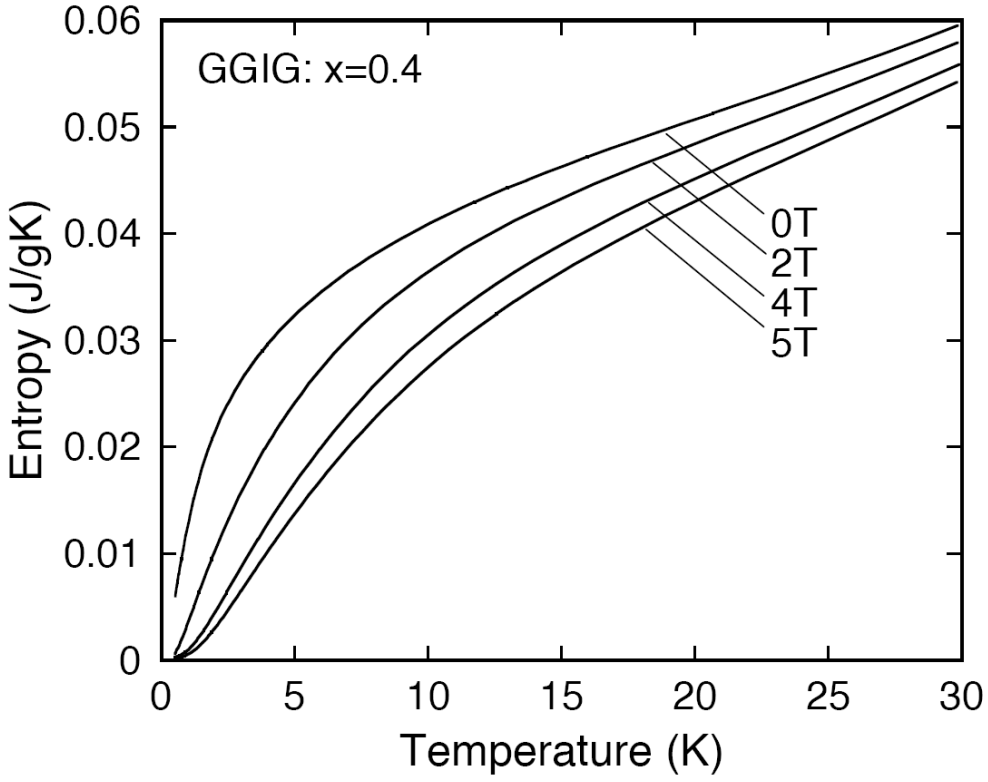

Figure 8: Entropy diagram for GGIG with x = 0.4 in 0, 2, 4, and 5 T [63].

Gadolinium Dysprosium Gallium Iron Garnet (GDGIG, chemical formula $(Gd_{0.5}Dy_{0.5})_3(Ga_{0.875}Fe_{0.125})_5O_{12}$) was studied in polycrystalline form [64]. The substitution of Gd with Dy in GGIG has enhanced the entropy change in small magnetic fields and at high temperatures in a similar way as the same substitution in GGG.

Dysprosium Gallium Garnet (DGG) is part of the family of antiferromagnetic rare earth garnets. Unlike Gd based garnets, which are only effective refrigerants below 15 K because they have little magnetic entropy change above that temperature, Dy still has a large magnetic entropy above 15 K and so Dy based garnets like DGG can be used up to at least 30 K [65]. DGG has a magnetic ordering temperature around 0.6 K, so it is most useful as a high temperature refrigerant [66]. The salt can be grown using the Czochralski process with the starting materials Dy_2O_3 and Ga_2O_3, which are both readily available from commercial chemical suppliers [65]. DGG has been the

subject of much study. Its heat capacity was measured by Tomokiyo et al. and Kimura et al. [65, 67]. Its thermal conductivity has been measured by [68]. The thermal conductivity of DGG features an interesting dependence on the magnetic field, shown in Figure 9 [69]. Strong phonon scattering is induced by the magnetic field and changes the thermal conductivity by up to a factor of 70.

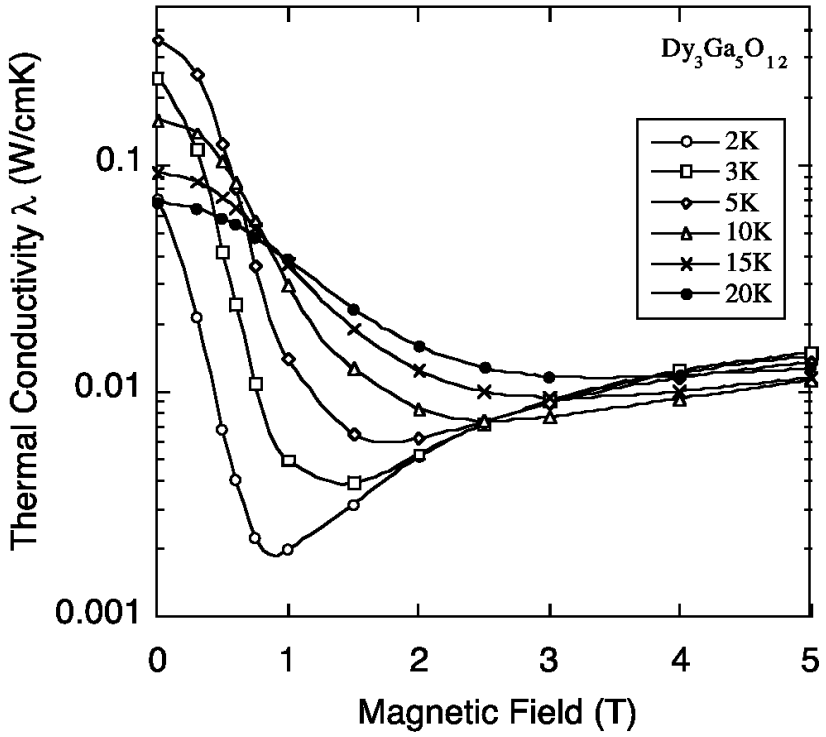

Figure 9: Magnetic field dependence of the thermal conductivity of DGG [69]

Gadolinium Lithium Fluoride (GLF, $GdLiF_4$) is an attractive material in that it has an ion desity somewhat higher than that of GGG and a transition temperature below 0.3 K [70, 71, 72]. Unfortunately, absolute values of the entropy as a function of temperature and field have not been published for this material. Figure 10 shows the magnetic entropy change of polycrystalline GLF, compared with that of GGG. The entropy change of GLF is 20 to

60 percent larger than the entropy change of GGG. A number of groups have successfully grown large crystals of this material, although usually doped with other rare earth ions for use in lasers.

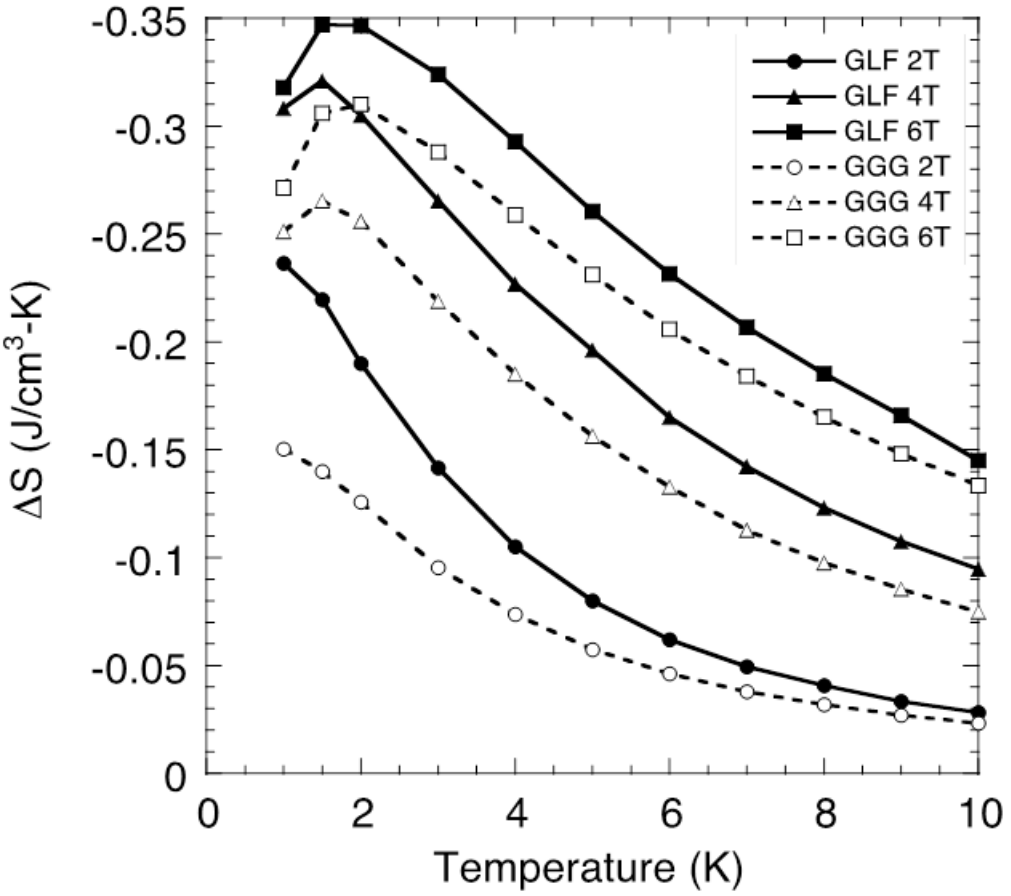

Figure 10: Entropy change of a GLF ($GdLiF_4$) polycrystalline sample and a GGG ($Gd_3Ga_50_{12}$) single crystal sample as functions of the magnetic field and temperature [71]. The mass density for GLF is 5.34 g/cm^3, and for GGG 7.08 g/cm^3.

Gadolinium Fluoride (GdF_3) has a gadolinium ion density 65.6 percent that of pure gadolinium, which among dielectric compounds is second only to gadolinium oxide. Its ordering temperature, 1.25 K, is much lower than that of Gd_2O_3 (3.8 K). Full entropy-temperature curves are presented for fields up to 5 T in DiPirro [72]. Unfortunately, GdF_3 appears to undergo a phase change, with significant volume change, upon cooling from melting

temperature, which makes the growth of large crystals very difficult. However, there is some evidence that this phase change is due to the presence of oxide impurities, and a few groups have successfully grown large single crystals by taking great care to eliminate these impurities [73].

3.3. Laves Phase Materials

Ferromagnetic materials are required in order to achieve magnetic entropy changes ΔS which are sufficiently large for refrigeration above 15 K, where the thermal energy of the phonons becomes large compared to the energies of the Zeeman levels in an external magnetic field of several Tesla. Especially in regenerative magnetic refrigeration, it is essential that the ordering temperature of the regenerator material is closely matched to the refrigerator's operating temperature range. As a consequence, a number of different magnetocaloric materials is required. Several studies have been performed on magnetic refrigerants in the temperature range above 20 K [74]. In this section, we focus on Laves phase materials.

Because of their large magnetic moments of about 10 μ_B per rare earth ion, RM_2 (R: rare earth; M: Al, Ni, Co) Laves phase rare earth intermetallic compounds with a cubic $MgCu_2$ structure have been studied and were found to have large magnetocaloric potentials and suitable transition temperatures for hydrogen liquefaction [75, 76]. The transition temperatures can be adjusted by changing the rare earth element R and/or the metal M; the nature of the phase transition differs among these compounds. The magnetic transition temperatures in the RM_2 system have a strong relation to the de Gennes factor G of the lanthanide ion:

$$G = (g-1)^2 \cdot J \cdot (J+1). \tag{25}$$

In Figure 11, the magnetic phase transition temperatures are shown as functions of the de Gennes factor for various RNi_2, RAl_2, and RCo_2 compounds [75, 77]. The transition temperature T_c of a single lanthanide compound scales almost linearly with the de Gennes factor. In compounds with two lanthanide ions, the partial substitution of one magnetic lanthanide with another one modifies the phase transition temperature, which is also shown in Figure 11. Changing the ratio of the rare earth elements can thus be used to tune the properties of a magnetic refrigerant to a particular temperature range.

RNi_2 and RAl_2 compounds have a second order phase transition from the paramagnetic to the ferromagnetic state. The specific heat of $ErAl_2$ is

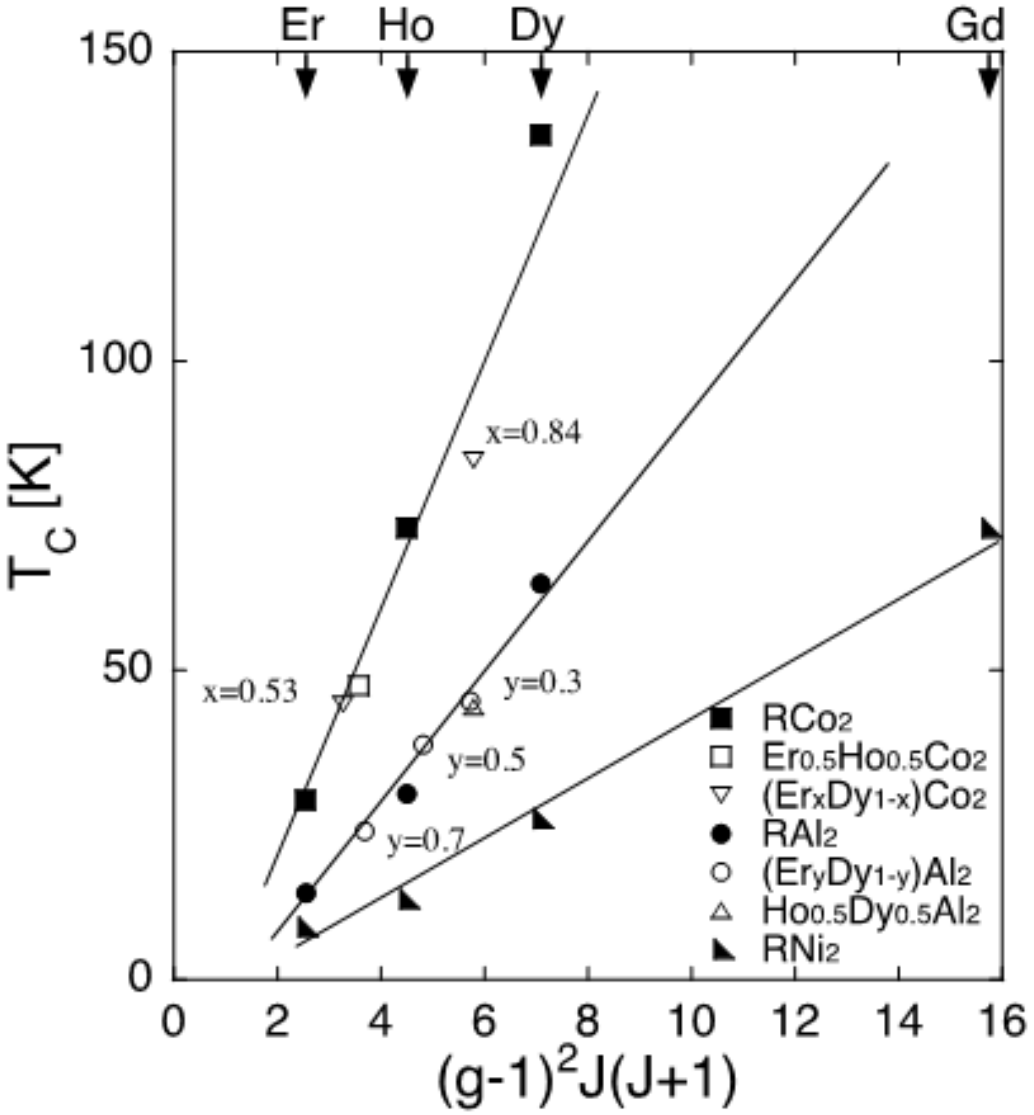

Figure 11: Magnetic phase transition temperatures for various RM_2 (M: Ni, Al, Co) compounds as a function of the de Gennes factor.

shown in Figure 12. RCo_2 compounds (R: Dy, Ho, and Er) feature intriguing magnetic properties [78] that result from interactions of localized 4f electrons and the itinerant 3d electrons of Co. Dy-, Ho- and Er-based RCo_2 compounds exhibit first-order paramagnetic-ferrimagnetic phase transitions,

while the others show second-order phase transitions from para- to ferromagnetic states. Above the transition temperature, a field-induced metamagnetic transition occurs.

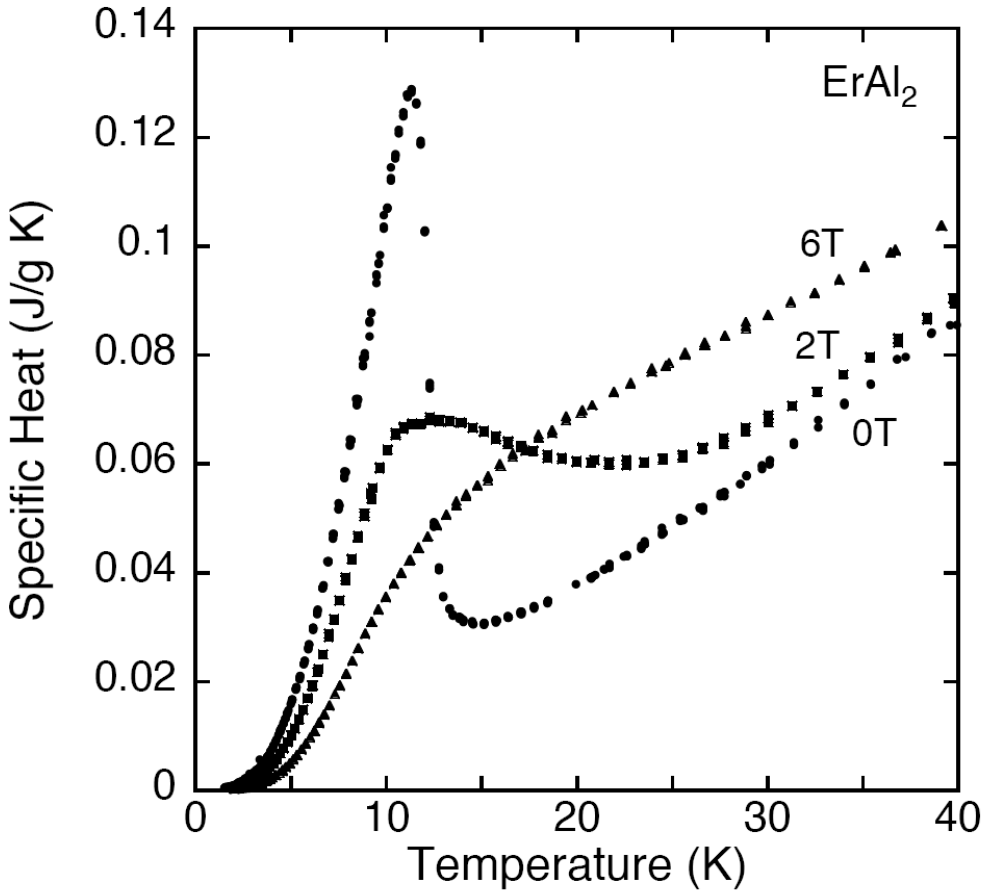

Figure 12: The specific heat of $ErAl_2$.

It has been shown that the substitution of Dy, Ho or Er with nonmagnetic Y ions (which yields $R_{1-x}Y_xCo_2$), and the substitution of Ho with Tb (which yields $Ho_{1-x}Tb_xCo_2$) can be used to control the transition temperature [79, 80]; however the substitution results in a change of the phase transition from first order to second order [81].

The magnetic transition temperature of RM_2 compounds can also be tuned by the substitution of M. For example, the magnetocaloric effect of $Ho(Co_{1-x}Ni_x)_2$ was studied by Wada et al. [82].

The effect of Er substitution in $Er_xHo_{1-x}Co_2$ and $Er_xDy_{1-x}Co_2$ has been studied in detail as the phase transition remains of first order in these systems. Figure 13 shows the specific heat of $(Er_{0.53}Ho_{0.47})Co_2$ as an example.

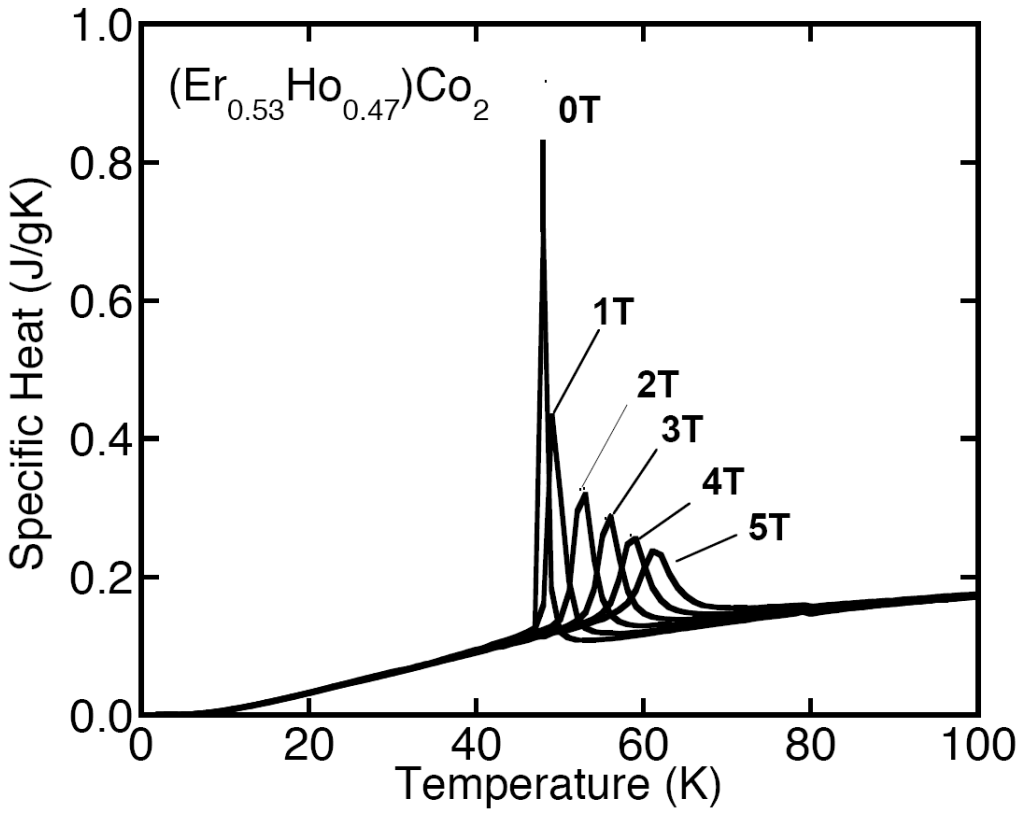

Figure 13: The specific heat of $(Er_{0.53}Ho_{0.47})Co_2$ [77].

Figure 14 shows the isothermal entropy change ΔS of several RM_2 compounds. ΔS has a peak around T_c and gradually decreases both above and below the transition temperature. ΔS of these compounds increases with increasing field and shows no saturation at least up to 5 T. Figure 14 illustrates how all RCo_2 compounds clearly show characteristics of a first-order transition. ΔS has a trapezoid shape formed by a sharp onset at T_c and a shoulder-like drop with increasing temperature. The maximum value of ΔS changes only slightly when the magnetic field is increased above 3 T. The temperature of the peak of ΔS moves to higher temperatures with increasing magnetic field, since the metamagnetic transition temperatures increases

with increasing magnetic field. As a consequence, refrigerators using RCo_2 materials have a larger cooling power density, but a narrower range of operating temperatures compared to RAl_2 and RNi_2.

Due to the complicated temperature and field dependence of the entropies of RM_2 compounds, numeric thermal modeling and cycle simulation are required to design and operate efficient AMRs with these materials.

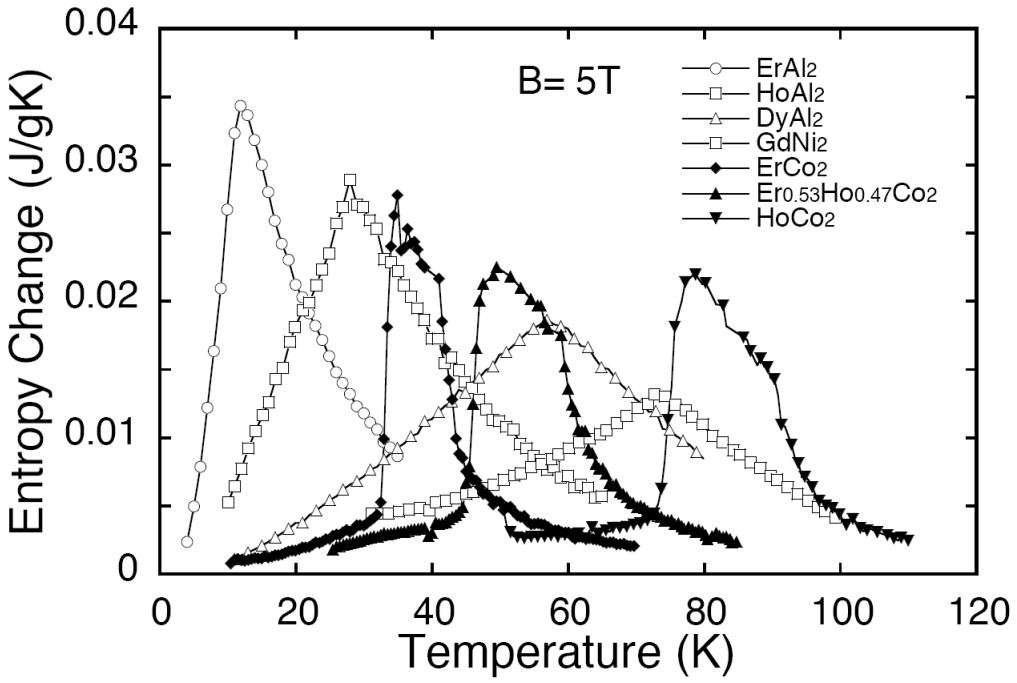

Figure 14: Entropy changes ΔS of various RM_2 materials in an external field of 5 T. ΔS was obtained from magnetization measurements.

In magnetic refrigerators, high cycle frequencies can be achieved either by using refrigerants with a high thermal conductivity, or by shaping the refrigerant such that the thermal penetration depth is on the order of the characteristic dimension of the refrigerant. Figure 15 shows the thermal conductivity of cast and sintered $DyAl_2$ samples, which is comparable to the rather poor thermal conductivity of stainless steel. As a consequence, shapes such as small spheres or thin sheet material are typically used for the construction of regenerators. Centrifugal atomization is used for $HoAl_2$, $DyAl_2$, and $GdNi_2$. Two representative examples of spherical compounds, $GdNi_2$ and

$DyAl_2$, are shown in Figure 16. Pellets of these materials exhibit sharp magnetic transitions and have good potential for use in magnetic refrigeration [83].

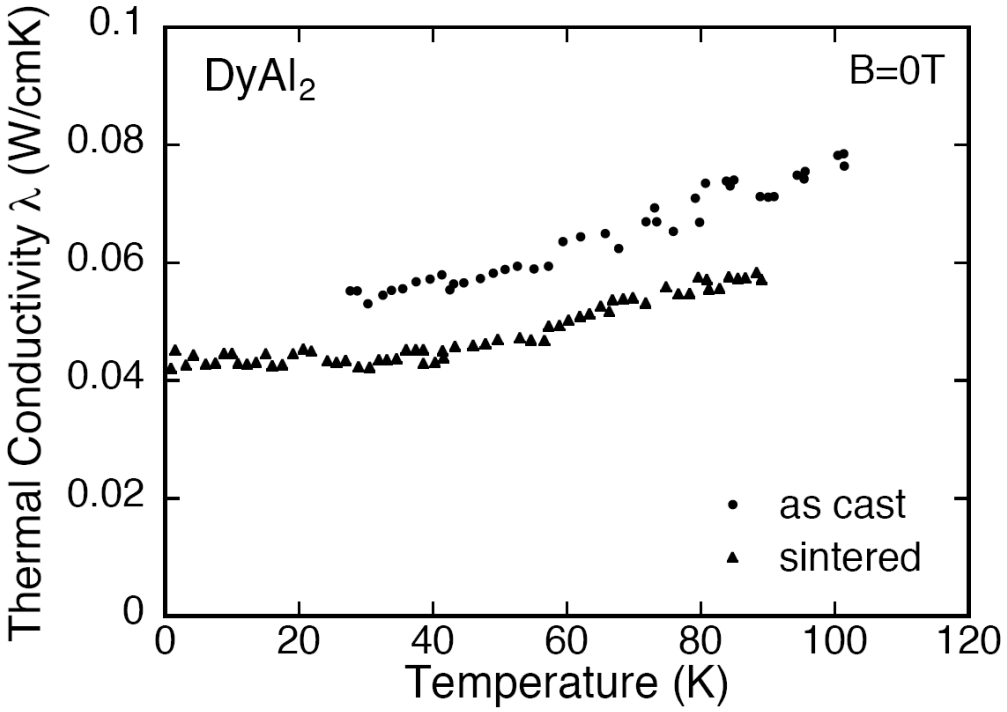

Figure 15: The thermal conductivity of cast and sintered $DyAl_2$ samples.

4. REFRIGERANT STAGE DESIGN CONSIDERATIONS

The choice of refrigerant has a strong impact on the details of the design of its enclosure, and how thermal contact is made to the refrigerant. McCammon and Shirron discuss the intricacies of constructing salt pills in [84]. Hydrated refrigerants, for instance, need to be sealed in a hermetic container to avoid de-hydration in the insulation vacuum of a cryostat. Another important point is material compatibility, especially with respect to corrosion.

In the following, another important design aspect - namely the thermal contact to the refrigerant - will be discussed in more detail, especially in view of its impact on a system's cooling power density. A good thermal

Table 1: Physical properties for some common paramagnetic refrigerants used in ADR (Carnot) cycles.

Refrigerant	Chemical Composition	J [1]	g [1]	T_o [K]	N [cm^{-3}]	S(0,T) [Ref]
CMN	$Ce_2Mg_3 \cdot (NO_3)_{12} \cdot 24H_2O$	1/2	2	0.0015	$1.65 \cdot 10^{21}$	[42]
CCA	$CrCs(SO_4)_2 \cdot 12H_2O$	3/2	2	0.01	$2.09 \cdot 10^{21}$	[87]
CPA	$CrK(SO_4)_2 \cdot 12H_2O$	3/2	2	0.009	$2.21 \cdot 10^{21}$	[48]
FAA	$Fe(SO_4)_2NH_4 \cdot 12H_2O$	5/2	2	0.026	$2.14 \cdot 10^{21}$	[48]
MAS	$Mn(SO_4)_2(NH_4)_2 \cdot 6H_2O$	5/2	2	0.17	$2.79 \cdot 10^{21}$	[48]
DGG	$Dy_3Ga_5O_{12}$	15/2 [a]	8	400	$1.28 \cdot 10^{22}$	[66]
GGG	$Gd_3Ga_5O_{12}$	7/2	2	0.38	$1.26 \cdot 10^{22}$	[36]
GLF	$GdLiF_4$	7/2	2	0.48	$1.34 \cdot 10^{22}$	[89]

[a] Below 1 K, the magnetic spin of DGG can be better approximated with $J = 1/2$ [88].

Table 2: Physical properties for some common paramagnetic refrigerants used in AMR cycles. Due to their anisotropy and temperature dependence, values for J and g are not listed in this table.

Refrigerant	Chemical Composition	T_o [K]	ΔS_{max} [J/(g · K)]	ρ [g/cm^3]	[Ref]
DAG (single crystal)	$Dy_3Al_5O_{12}$	2.4	0.011 (20 K, 6 T)	-	[54]
DAG (polycrystalline)	$Dy_3Al_5O_{12}$	2.4	0.0098 (20 K, 6 T)	-	[54]
GDAG	$(Gd_xDy_{1-x})_3Al_5O_{12}$	1.58	0.013 (20 K, 6 T)	-	[54]
GGIG	$Gd_3(Ga_{1-x}Fe_x)_5O_{12}$	0.81	0.0062 (20 K, 5 T)	-	[63]
GDGIG	$(Gd_{0.5}Dy_{0.5})_3(Ga_{0.875}Fe_{0.125})_5O_{12}$	0.85	0.007 (20 K, 5 T)	-	[64]
GdF	GdF_3	1.25	0.026 (10 K, 5 T)	7.047	[72]
$ErAl_2$		12	0.034 (T_o, 5 T)	6.2	[75]
$HoAl_2$		28	0.029 (T_o, 5 T)	6.1	[75, 83]
$DyAl_2$		63	0.019 (T_o, 5 T)	5.9	[75, 83]
$GdNi_2$		75	0.013 (T_o, 5 T)	10.2	[83]
$ErCo_2$		37	0.026 (T_o, 5 T)	10.3	[38, 76, 77]
$HoCo_2$		83	0.022 (T_o, 5 T)	10.2	[38, 76, 77]

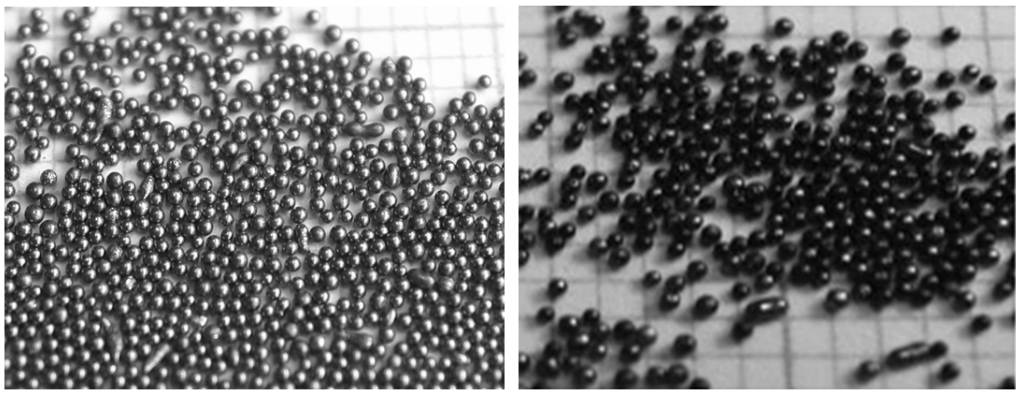

Figure 16: Photograph of spherical RM_2 compounds [83]. Left: $GdNi_2$ with a particle size of 355-500 μm. Right: $DyAl_2$ with a particle size of 355-500 μm.

contact between the refrigerant and the sample to be cooled is required to achieve high thermodynamic efficiency, both in steady state (the lower the temperature gradient between the refrigerant and the sample, the higher the COP) and during transient conditions (high COPs can only be achieved if a system's thermalization time is short compared to the characteristic cycle time).

The thermal conductivity of dielectric salts is on the order of 10^{-2} W/(K $\cdot$ m) at 0.1 K [13]. As a consequence, the thermal path in the salt must be minimized, and crystals of these materials are often grown around heat busses made of bundles of highly conductive metal wires. Figure 17 shows such a heat bus made from gold wires, which has been used for the construction of an FAA salt pill. Figure 18 shows a different design which has been devised at NASA GSFC for CPA salt pills.

To optimize the design, the size of the metal structure providing the thermal conductivity has to be traded off against the lost salt volume. In a simplified thermal model of a refrigerant pill, shown in Figure 19, the steady state heat flux through the heat bus into the refrigerant at temperature T_R can be calculated from the following differential equation:

$$\frac{d^2T(x)}{dx^2} = \frac{\alpha \cdot \beta}{\lambda \cdot A_{HB}} \cdot (T(x) - T_R), \tag{26}$$

where α characterizes the boundary resistance between the heat bus and the refrigerant, β is the contact area between the heat bus and the refrigerant

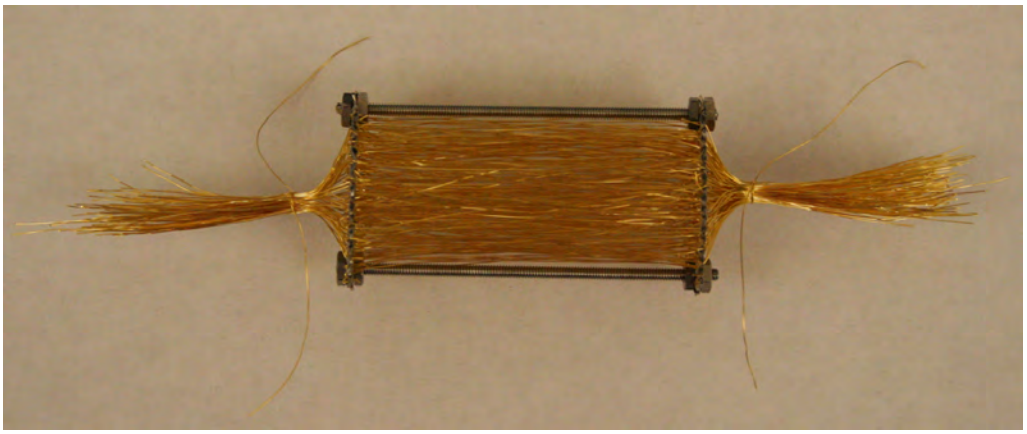

Figure 17: A heat bus made from a bundle of gold wires around which FAA crystals were grown for the salt pill of the ADR for the Micro-X sounding rocket telescope [85]. The gold wires ensure good thermal contact between the salt crystals and the two heat busses of the salt pill.

per unit length, λ the thermal conductivity of the heat bus material and A_{HB} the cross section of the heat bus.

With the boundary conditions that $T(x = 0) = T_{cold}$ and $\dot{Q}(x = l) = 0$, one obtains the following solution for the temperature profile in the heat bus:

$$T(x) = T_R + \frac{T_{cold} - T_R}{1 + e^{2ml}} \cdot (e^{mx} + e^{2ml} \cdot e^{-mx}), \tag{27}$$

where

$$m = \sqrt{\frac{\alpha \cdot \beta}{\lambda \cdot A_{HB}}}. \tag{28}$$

The total heat flux from the heat bus into the refrigerant is

$$\dot{Q}(x = 0) = -\lambda \cdot A_{HB} \cdot \left(\frac{dT}{dx}\right)_{x=0} = \\ = -\lambda \cdot A_{HB} \cdot \frac{m \cdot (T_{cold} - T_R)}{1 + e^{2ml}} \cdot (1 - e^{2ml}). \tag{29}$$

The total amount of heat Q that can be absorbed at the temperature T_{cold} is proportional to the product of the amount of refrigerant $(A_{tot} - A_{HB}) \cdot l$

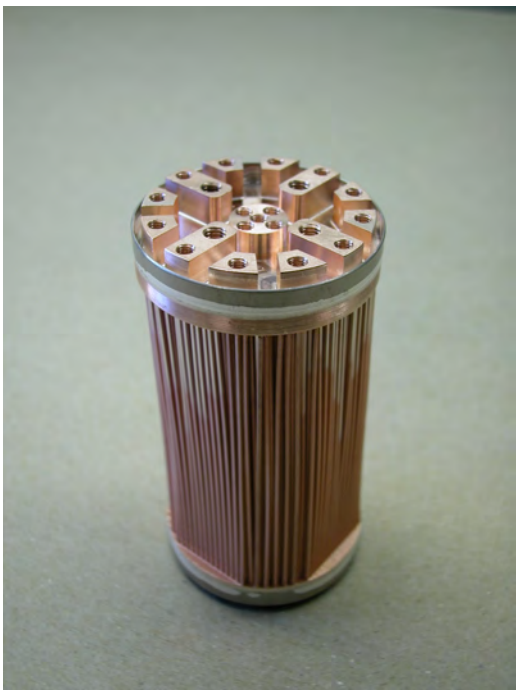

Figure 18: A copper heat bus for a CPA salt pill which was built at the NASA Goddard Space Flight Center. As CPA is not as corrosive as FAA, the heat bus for CPA salt pills can be constructed from copper. The copper part was manufactured with an Electrical Discharge Machining (EDM) process. A stainless steel sleeve is welded around the copper heat bus before the crystals are grown.

and the total heat flux $\dot{Q}$ into the refrigerant for a given combination of T_{cold} and T_R. The maximum of Q can be obtained by differentiation with respect to A_{HB}.

The fluorides and oxides which are used as magnetocaloric refrigerants at higher temperatures (such as GGG or GLF) can often be grown as large single crystals. The thermal conductivity is on the order of 10 W/(K $\cdot$ m) at 3 K and 100 W/(K $\cdot$ m) at 10 K [86], and no special measures need to be taken to enhance the thermal contact to the refrigerant. Very often, fluoride and oxide refrigerants are simply sealed in sintered or powdered form into hermetic containers with some exchange gas.

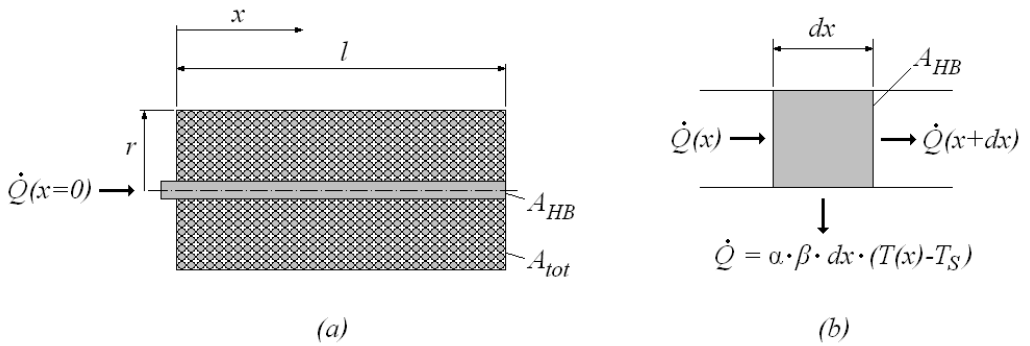

Figure 19: A simplified model of a refrigerant pill. In this model, the refrigerant has infinite thermal conductivity in the radial direction, and zero thermal conductivity in the axial direction. Axial heat conduction occurs only in the heat bus. In a real refrigerant pill, a large number of metal wires is used instead of one single rod to approximate this idealized model.

5. CONCLUSION

In cryogenics, magnetic refrigeration remains the most suitable technology for many applications. In most cases, magnetic refrigeration systems are optimized such that the volume of the refrigerant is minimal. In this paper, we have reviewed the most important properties of magnetic refrigerants which influence cooling power density, followed by a description of the magnetocaloric materials most commonly used in low temperature applications (paramagnetic salts, rare-earth oxides and fluorides, and Laves-phase materials).

References

[1] Knuuttila T. (2000). Nuclear Magnetism and Superconductivity in Rohdium. Helsinki University of Technology, Espoo, Finland.

[2] Brown G.V. (1976). J. Appl. Phys. 47, 3673.

[3] Yu B.F., Gao Q., Zhang B., Meng X.Z. and Chen Z. (2003). Int. J. of Refrig. 26, 622.

[4] Shirron P. (2013). This issue. "Overview of magnetocaloric effect and architectures".

[5] Ambler E. and Hudson R.P. (1955). Rep. Prog. Phys. 18, 251.

[6] Kelley, R.L., Audley, M.D., Boyce, K.R., Fujimoto, R., Gendreau, K.C., Ishisaki, Y., McCammon, D., Mihara, T., Mitsuda, K., Moseley, S.H., Mott, D.B., Porter, F.S., Stahle, C.K. and Szymkowiak, A.E. (2000). Nucl. Instr. and Meth. Phys. Res. 444, 170-174.

[7] Kelley, R.L., Mitsuda, K., Allen, C.A., Arsenovic, P., Audley, M.D., Bialas, T.G., Boyce, K.R., Boyle, R.F., Breon, S.R., Brown, G.V., Cottam, J., Dipirro, M.J., Fujimoto, R., Furusho, T., Gendreau, K.C., Gochar, G.G., Gonzalez, O., Hirabayashi, M., Holt, S.S., Inoue, H., Ishida, M., Ishisaki, Y., Jones, C.S., Keski-Kuha, R., Kilbourne, C.A., McCammon, D., Morita, U., Moseley, S.H., Mott, B., Narasaki, K., Ogawara, Y., Ohashi, T., Ota, N., Panek, J.S., Porter, F.S., Serlemitsos, A., Shirron, P.J., Sneiderman, G.A., Szymkowiak, A.E., Takei, Y., Tveekrem, J.L., Volz, S.M., Yamamoto, M. and Yamasaki, N.Y. (2007). Publications of the Astronomical Society of Japan 59, 77-112.

[8] Shirron P. (2013). This issue. "Optimization of single- and multi-stage ADRs".

[9] Matsumoto K., Kondo T., Yoshioka S., Kamiya K. and Numazawa T. (2009). J. of Phys. 150, 012028.

[10] Zimm C., Jastrab A., Sternberg A., Pecharsky V., Gschneidner K., Osborne M. and Anderson I. (1998). Adv. Cryo. Eng. 43, 1759.

[11] Rowe A. (2013). This issue. "AMR, theory".

[12] Matsumoto K. (2013). This issue. "Ultra-low temperature: nuclear demag"

[13] Pobell F. (1995). Matter and Methods at Low Temperatures. Springer, Berlin.

[14] Enss C. and Hunklinger S. (2005). Low-Temperature Physics. Springer, Berlin.

[15] Hepburn I.D. and Smith A. (1999), in Webster J. (ed), Wiley Encyclopedia of Electrical and Electronics Engineering. John Wiley and Sons, Inc.

[16] Feynman R.P., Leighton R.B., Sands M. (1964, 1966). The Feynman Lectures on Physics. Library of Congress Catalog Card No. 63-20717.

[17] Rowe A. (2012). Cryogenics 52, 111.

[18] Rowe A. (2012). Cryogenics 52, 119.

[19] McCammon D. (2013). This issue. "Suspension Systems"

[20] Yu, B.F., Gao, Q., Zhang, B., Meng, X.Z. and Chen, Z. (2003), International Journal of Refrigeration 26, 622-636.

[21] Wood M.E. and Potter W.H. (1985). Cryogenics 25, 667.

[22] Hund F. (1927). Zeitschrift fr Physik. 40, 742.

[23] Hund F. (1927). Zeitschrift fr Physik. 42, 93.

[24] Kramers, H. A. (1930). Proc. Amsterdam Acad. 33, 959.

[25] Finn C.B.P., Orbach R. and Wolf W.P. (1961). Proc. Phys. Soc. 77, 261.

[26] Blundell S. (2001). Magnetism in Condensed Matter. Oxford University Press.

[27] Rotter M. (2003). Magnetic Properties of Gadolinium Compounds. Habilitation, Technische Universitt Dresden.

[28] Kuzmin M.D. and Tishin A.M. (1993). J. Appl. Phys. 73, 4083.

[29] Ruderman M.A. and Kittel (1954). Phys. Rev. 96, 99.

[30] Kasuya T. (1956). Prog. Theor. Phys. 16, 45.

[31] Yosida K. (1957). Phys. Rev. 106, 893.

[32] Roser M.R., Jingchun Xu, White S.J., Corruccini L.R. (1992). Phys. Rev. B 45, 12337.

[33] Torres F., Hernndez J.M., Bohigas X., and Tejada J. (2000). Appl. Phys. Lett. 77, 3248.

[34] Ramirez A.P. and Kleiman R.N. (1991). J. Appl. Phys. 69, 5252.

[35] Petrenko O.A., McK Paul D., Ritter C., Zeiske T., Yethiraj M. (1999). Physica B 266, 41.

[36] Schiffer P., Ramirez A.P., Huse D.A. and Valentino A.J., Phys. Rev. Lett. 73 (1994), 2500.

[37] Zhitomirsky M.E. (2003). Phys. Rev. B 67, 104421.

[38] Pecharsky V.K. and Gschneidner K.A. (1997), Phys. Rev. Lett. 78, 44944497.

[39] Gschneidner K.A., Pecharsky V.K. and Tsokol A.O. (2005). Rep. Prog. Phys. 68, 14791539.

[40] Mess K.W., Niesen L. and Huiskamp W.J. (1970). Physica 45, 626.

[41] Giauque W.F., Fisher R.A., Hornung E.W and Brodale G.E. (1973). J. of Chem. Phys. 58, 2621.

[42] Fisher R.A., Hornung E.W., Brodale G.E. and Giauque W.F. (1973). J. of Chem. Phys. 58, 5584.

[43] Hudson R.P. (1972). Principles and Application of Magnetic Cooling. North-Holland, Amsterdam.

[44] Abel W.R., Anderson A.C., Black W.C. and Wheatley J.C. (1966). Phys. Rev. Letters 16, 273.

[45] Frossati G., Hebral B., Schumacher G. and Thoulouze D (1977). Physica 90B, 61.

[46] Betts D.S. (1976). Refrigeration and Thermometry Below One Kelvin. Sussex University Press, London.

[47] de Haas W.J., Wiersma E.C., Kramers H.A. (1933). Physica 1, 1.

[48] Vilches O.E. and Wheatley J.C. (1966). Rev. Sci. Instr. 37, 819.

[49] Vilches O.E. and Wheathley J.C. (1966). Phys. Rev. 148, 509.

[50] Kapadnis D.G. (1956). Physica 22, 159.

[51] Barclay J.A. and Steyert W.A. (1982). Cryogenics 22, 73.

[52] Hakuraku Y. and Ogata H. (1986). Jpn. J. Appl. Phys. 25, 140.

[53] Fisher R.A., Brodale G.E., Hornung E.W. and Giauque W.F. (1973). J. Chem. Phys. 59, 4652.

[54] Numazawa T., Kamiya K., Abe S. and Matsumoto K. (2004). Proceedings WHEC 15.

[55] Slack G.A. and Oliver D.W. (1971). Phys. Rev. B 4, 592.

[56] Numazawa T. and Sato A. (1999). Proc. ICEC 17, 287.

[57] Numazawa T., Kamiya K., Yoshioka S., Nakagome H. and Matsumoto K. (2008). AIP Conference Proceedings 986, 1183.

[58] Matsumoto K., Kondo T., Yoshioka S., Kamiya K. and Numazawa T. (2009). J. of Phys. Conference Series 150, 012028.

[59] Numazawa T., Kamiya K., Yoshioka S., Nakagome H. and Matsumoto K. (2008). AIP Proc. 985, 1183.

[60] McMichael R.D., Ritter J.J. and Shull R.D. (1993). J. Appl. Phys. 73, 6946.

[61] Provenzano V., Li J., King T., Canavan E., Shirron P., DiPirro M. and Shull R.D (2003). J. Magn. Magn. Mater. 266, 185.

[62] McMichael R.D., Shull R.D., Swartzendruber L.J., Bennett L.H. and Watson R.E. (1992). J. Magn. Magn. Mater. 111, 29.

[63] Matsumoto K., Matsuzaki A., Kamiya K. and Numazawa T. (2009). Jpn. J. Appl. Phys. 48, 113002.

[64] Matsumoto K., Okano T., Matsuzaki A., Kamiya K. and Numazawa T. (2003). Physica B, 329, 1261.

[65] Kimura H., Maeda H. and Sato M., J. of Mat. Sci. 23 (1988), 809.

[66] Goshorn D.P., Onn D.G. and Remeika J.P., Phys. Rev. B 15 (1977), 3527.

[67] Tomokiyo A., Yayama H., Hashimoto T., Aomine T., Nishida M. and Skaguchi S. (1985). Cryogenics 25, 271.

[68] Numazawa T., Kimura H., Sato A., Maeda H., Shimamura K. and Fukuda T., Adv. Cryog. Eng. 42 (1996), 459.

[69] Numazawa T., Kimura H., Sato M., Sato H., Shimamura K. and Fukuda T. (1997). Proc. ICEC 16, 2073.

[70] Shirron P., Canavan E., DiPirro M., Francis J., Jackson M., Tuttle J., King T. and Grabowski M. (2003). Cryogenics 44, 581.

[71] Numazawa T., Kamiya K., Shirron P., DiPirro M. and Matsumoto K. (2006). AIP Conf. Proc. 850, 1579.

[72] DiPirro M., Canavan E., Shirron P. and Tuttle J. (2004). Cryogenics 44, 559.

[73] Walker P.J. (1981). Progress in Crystal Growth and Characterization 33, 103.

[74] Tishin A.M. and Spichkin Y.I. (2003). IOP Puslishing, ISBN 0-7503-0922-9

[75] Hashimoto T., Matsumoto K., Kurihara T., Numazawa T., Tomokiyo A., Yayama H., Goto T. and Sahashi M., (1986). Adv. Cryo. Eng. 32, 279.

[76] Matsumoto K., Kouen T., Nishida R., Abe S., Kamiya K. and Numazawa T., (2006). AIP Conference Proceedings 850, 1581.

[77] Zhu Y., Asamoto K., Nishimura Y., Kouen T., Abe S., Matsumoto K. and Numazawa T. (2011). Cryogenics 51, 494.

[78] Nikitin S.A. and Tishin A.M. (1991). Cryogenics 31, 166.

[79] Wada H., Tomekawa S. and Shiga M. (1999). Cryogenics 39, 915.

[80] Pillmayr C, Schmitzer E, Gratz G, Hilscher and Sechovsky V. (1987). J. Magn. Magn. Mater. 70, 162.

[81] Herrero-Albillos J., Bartolome F., Garcia L.M., Casanova F., Labarta A. and Batlle X. (2006). Phys Rev B 73, 134410.

[82] Wada H., Tanabe Y., Shiga M., Sugawara H. and Satob H. (2001). Journal of Alloys and Compounds 316, 245.

[83] Matsumoto K., Asamato K., Nishimura Y., Zhu Y., Abe S. and Numazawa T. (2012). Journal of Physics: Conference Series 400, 052020.

[84] McCammon D. and Shirron P. (2013). This issue. "Salt pill design and fabrication".

[85] Wikus P., Rutherford J.M., Trowbridge S.N., McCammon D., Adams J.S., Bandler S.R., Das R., Doriese W.B., Eckart M.E., Figueroa-Feliciano E., Kelley R.L., Kilbourne C.A., Leman S.W., Porter F.S. and Sato K. (2010). Cryocoolers 16, 547.

[86] Slack G.A. and Oliver D.W. (1971). Phys. Rev. B 42, 592.

[87] Hagmann C., Benford D.J. and Richards P.L., Cryogenics 34 (1994), 213.

[88] Shirron P.J., Canavan E.R., DiPirro M.J., Tuttle J.G. and Yeager C.J., Advances in Cryogenic Engineering 45 (1999), 1629.

[89] Numazawa T., Kamiya K., Shirron P., DiPirro M. and Matsumoto K., AIP Conference Proceedings 850 (2006), 1579.